Sensitivity Analysis of Biochemical Systems Using Bond Graphs

Peter J. Gawthrop [*1] and Michael Pan [1,2]

[1] Systems Biology Laboratory, School of Mathematics and Statistics, and Department of Biomedical Engineering, University of Melbourne, Victoria 3010, Australia.
[2]School of Mathematics and Statistics, Faculty of Science, University of Melbourne, Victoria 3010, Australia

April 4, 2023

Abstract

The sensitivity of systems biology models to parameter variation can give insights into which parameters are most important for physiological function, and also direct efforts to estimate parameters. However, in general, kinetic models of biochemical systems do not remain thermodynamically consistent after perturbing parameters. To address this issue, we analyse the sensitivity of biological reaction networks in the context of a bond graph representation. We find that the parameter sensitivities can themselves be represented as bond graph components, mirroring potential mechanisms for controlling biochemistry. This approach naturally extends to finding sloppy parameters in biological models. We verify our approach using a model of the Pentose Phosphate Pathway, confirming the reactions and metabolites most essential to maintaining the function of the pathway.

[*]Corresponding author. **peter.gawthrop@unimelb.edu.au**

1 Introduction

The *sensitivity* of a system is a quantitative measure of how much system outputs change in response to changes in parameters or inputs; a system that is insensitive is said to be *robust*. On the other hand, parameters associated with high sensitivity are often important for the function of a biological system, for example defining switch-like behaviours [1]. Sensitivity theory of dynamical systems and its application to engineering systems is well established and summarised in the textbooks [2, 3]. There are many applications of sensitivity methods to systems and control problems including: system optimisation, control system analysis [4, 5] controller tuning [6] and parameter estimation [7, 8].

The importance of sensitivity to the discipline of Systems Biology has long been recognised [9–12] and continues to be investigated [13–15]. In particular, Metabolic Control Analysis (MCA) [16–20] applies sensitivity methods to the analysis of chemical reaction networks in general and metabolism in particular. A thorough investigation into the links between MCA and more general sensitivity theory can be found in the works of Ingalls [21–24].

Because of the overlap between Engineering and Systems Biology, it is insightful to import methods from the former to the latter [25–27]. The bond graph technique provides one example of this methodological transfer, and has shown great potential in constraining models to be consistent with the laws of physics and thermodynamics [28, 29]. Bond graphs were introduced by Paynter [30, 31] to model the flow of *energy* though physical systems of interest to engineers and are described in several text books [32–35] and a tutorial for control engineers [36]. Bond graphs provide a systematic approach to elucidating the *analogies* between disparate physical domains based on energy and thus can also provide a foundation for Systems Biology. In particular, bond graphs were first used to model chemical reaction networks by Katchalsky and coworkers [37]. A detailed account is given by Oster et al. [38] and an overview of the approach is given by Perelson [39]. This work has been extended to Systems Biology [28, 40–46].

Sensitivity analysis is often based on analysing the ODE derived from a system rather than the system itself [12, 15]. In contrast, this paper analyses the system itself following the bond graph approach to sensitivity analysis that has previously been developed for engineering systems [47–49]. This approach has the advantage that the sensitivity is with respect to physically-meaningful parameters and both unperturbed and perturbed systems obey basic physical laws such as mass and energy conservation.

A key insight in sensitivity analysis is that the sensitivity properties of a system may be described by a related system: the *sensitivity system* [2, 48–50]. This notion has been extended in the context of bond graph models of engineering systems to the idea that a system represented by a bond graph has a sensitivity system also described by a bond graph [48, 49]. As will be shown, this property is inherited by biochemical systems.

There are two main categories of sensitivity analysis: local and global [12]. The former corresponds to small parameter variations and leads to linear dynamic systems; the latter corresponds to large parameter variations [12, 15]. We focus on local sensitivity in this paper. Although the local approach is approximate, it is more computationally efficient than global methods and offers more insight into the effects of varying combinations of parameters. The variation of the local model properties with the point of linearisation can also give insight into system properties.

The local approach can also be for initial investigations followed by targeted global analysis [51]. Local sensitivity analysis is closely related to linearisation which has already been examined in the bond graph systems biology context [41, 52]; this paper explicitly shows this relationship. This paper looks at the approximation inherent in local analysis by comparing global with local results for a range of examples.

Sensitivity analysis can either be static and show how steady-state values of species depend on parameters, as in MCA , or be dynamic and show how the time trajectories of species depend on parameters. This paper looks at *dynamic* sensitivity analysis; this enables not only static values of sensitivity to be derived but also the sensitivity of the time course of species as parameters change. These sensitivity trajectories can be represented as a transfer function, the properties of which can be summarised in various ways according to the application. For example, the trajectory transfer function can be summarised by steady-state gain (also know as DC gain), initial response and time constant or, in the context of control theory, by a frequency response.

This paper extends bond graph based sensitivity analysis to biochemical systems. In particular, the bond graph of the sensitivity system of a biochemical system is derived; following [48], this involves ascertaining the sensitivity *component* associated with biochemical bond graph components. Biochemical systems form a subset of nonlinear systems with special properties. In particular, the mass-action equations result from the logarithmic nature of chemical potential [40, 53] and the exponential nature of the Marcelin – de Donder formulation of reaction flows [40, 54]. As will be shown, this leads to the reformulation of parametric variation in terms of modulating chemical potentials.

It is well known that system dynamics can be insensitive to variation of parameters: this behaviour has been called *Sloppy Parameter Sensitivities* [55]. In particular, a quadratic cost function involving system trajectories has been formulated [55] to investigate this behaviour. This paper draws explicit links with Sloppy Parameter analysis.

§ 2 gives the background in bond graph modelling required for the rest of the paper and introduces a set of normalised variables. § 3 introduces the bond graph sensitivity system appropriate to biochemical systems. § 4 shows how the nonlinear sensitivity system can be linearised. § 5 explores the relationship between the sensitivity system and the concept of sloppy parameter sensitivities. § 6 and § 7 look at two examples: a modulated enzyme-catalysed reaction and the Pentose Phosphate Pathway.

The Python code used to generate the Figures in this paper is available as Jupyter notebooks at `https://github.com/gawthrop/Sensitivity23`.

2 Bond graph modelling of biochemical systems

This section summarises the material needed for the rest of the paper. § 2.1 summarises, in the form of a specific example, the basic ideas of modelling biochemical systems to be found in more detail in a recent paper [28]. § 2.2 introduces a normalisation approach to simplify the sensitivity analysis and § 2.3 considers the stoichiometry of bond graph models [28]. § 2.4 summarises the linearisation of biochemical systems [41].

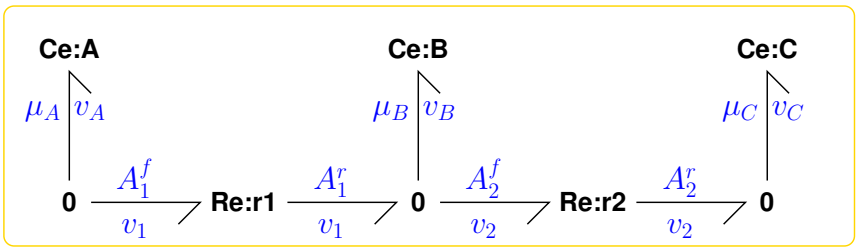

Figure 1: Example A $\overset{\mathrm{r}_1}{\rightleftharpoons}$ B $\overset{\mathrm{r}_2}{\rightleftharpoons}$ C. The three species A, B and C are represented by the three bond graph components **Ce**:A, **Ce**:B and **Ce**:C and the two reactions r_1 and r_2 by the two bond graph components **Re**:r1 and **Re**:r2. The bonds $\rightharpoonup$ carry the chemical potential μ, or affinities comprising sums of potentials, and molar flow v, and thus energy flows, between components. The **0** junctions combine energy flows in such a way the all impinging bonds carry the same potential.

2.1 Example: modelling the chemical reactions A $\rightleftharpoons$ B $\rightleftharpoons$ C

This example considers the two chemical reactions A $\overset{\mathrm{r}_1}{\rightleftharpoons}$ B $\overset{\mathrm{r}_2}{\rightleftharpoons}$ C where the substance A is inter-converted with substance C via the intermediate substance B. Figure 1 gives the corresponding Bond Graph which consists of: the *components* **Ce** and **Re** which represent species and reactions respectively, the *bonds* $\rightharpoonup$ which carry energy in the form of chemical potential μ $(\mathrm{J\,mol^{-1}})$ and molar flow v $(\mathrm{mol\,s^{-1}})$ whose product $\mu \times v$ has units of power $(\mathrm{J\,s^{-1}}$ or $\mathrm{W})$ and the **0** junction which connects bonds in such a way that all impinging bonds carry the same potential. Thus, for example $A_1^f = \mu_A$ and $v_A = -v_1$; similarly $A_1^r = A_2^f = \mu_B$ and $v_B = v_1 - v_2$. Although not used in Figure 1, the dual **1** junction connects bonds in such a way that all impinging bonds carry the same flow. **Ce** components store, but do not dissipate, energy; **Re** components dissipate, but do not store, energy; bonds and junctions transmit energy without storage or dissipation.

The **Ce**:A component has the constitutive equations

$$\mu_A = RT \ln K_A x_A \tag{2.1}$$

$$\text{where } \frac{dx_A}{dt} = v_A \tag{2.2}$$

Where the time derivative in (2.2) means that this component is dynamic. $R = 8.314\,\mathrm{J\,mol^{-1}\,K^{-1}}$ is the Universal Gas Constant and T (K) the absolute temperature. μ_A $(\mathrm{J\,mol^{-1}})$ is the chemical potential of substance A , x (mol) the amount of substance A and v_A $(\mathrm{mol\,s^{-1}})$ the molar flow of substance A.

In contrast, the **Re**:r1 component is static with constitutive equation

$$v_1 = \kappa_1 \left(\exp \frac{A_1^f}{RT} - \exp \frac{A_1^r}{RT} \right) \tag{2.3}$$

Where A_1^f $(\mathrm{J\,mol^{-1}})$ and A_1^r $(\mathrm{J\,mol^{-1}})$ are the forward and reverse affinities associated with reaction r_1 and v_1 $(\mathrm{mol\,s^{-1}})$ the molar flow associated with reaction r_1. Analogous equations apply to the **Ce** components B and C, and the **Re** component r_2.

In this simple example, these equations yield the well-known law of mass action

$$v_1 = \kappa_1 \left(\exp \ln K_A x_A - \exp \ln K_B x_B\right) = \kappa_1 \left(K_A x_A - K_B x_B\right) \tag{2.4}$$

$$\text{and } v_2 = \kappa_2 \left(\exp \ln K_B x_B - \exp \ln K_C x_C\right) = \kappa_2 \left(K_B x_B - K_C x_C\right) \tag{2.5}$$

More complex biochemical system are needed to reveal the full power of the bond graph approach. For example detailed balance and Wegscheider conditions are automatically satisfied [28, 56].

As discussed previously [28, 41], an open system can be obtained from a closed system by replacing dynamic **Ce** components by *chemostats* [57] where the ODE (2.2) is replaced by

$$x = x_e \tag{2.6}$$

This example is continued throughout the paper as an open system with both **Ce**:A and **Ce**:C chemostats. This corresponds to the situation where substrate A and product C are kept at constant amounts.

2.2 Normalisation

It is convenient to re-express chemical potential μ $(\mathrm{J\,mol^{-1}})$ in non-dimensional form $\boldsymbol{\phi}$ where

$$\boldsymbol{\phi} = \frac{\mu}{\mu_0} \text{where } \mu_0 = RT \approx 2.579 \ (\mathrm{kJ\,mol^{-1}}) \tag{2.7}$$

For this section, we derive numerical values assuming that $T = 37°\mathrm{C} \approx 310$ K. To re-express molar flow v $(\mathrm{mol\,s^{-1}})$ in non-dimensional form $\boldsymbol{f}$, define a normalising power P_0 (W). Choosing $P_0 = 1\,\mathrm{mW}$ gives

$$\boldsymbol{f} = \frac{v}{v_0} \tag{2.8}$$

$$\text{where } v_0 = \frac{P_0}{\mu_0} \approx 0.3878 \ (\mathrm{\mu mol\,s^{-1}}) \tag{2.9}$$

The amount x can be re-expressed as the normalised variable $\boldsymbol{x}$

$$\boldsymbol{x} = \frac{x}{x_0} \tag{2.10}$$

$$\text{where } x_0 = v_0 t_0 \tag{2.11}$$

where t_0 (s) is a normalising time unit and v_0 is given by (2.9). We can also define the normalised time as $\boldsymbol{t} = t/t_0$. Thus, the derivative $\frac{dx}{dt}$ of the amount x can be re-expressed as the normalised variable $\frac{d\boldsymbol{x}}{d\boldsymbol{t}}$:

$$\frac{d\boldsymbol{x}}{d\boldsymbol{t}} = \frac{t_0}{x_0}\frac{dx}{dt} = \frac{1}{v_0}\frac{dx}{dt} \tag{2.12}$$

Using normalised variables, the **Ce** constitutive relation (2.1) becomes:

$$\boldsymbol{\phi} = \ln \boldsymbol{K}\boldsymbol{x} \tag{2.13}$$

$$\text{where } \boldsymbol{K} = x_0 K \tag{2.14}$$

and the **Re** constitutive relation (2.3) becomes:

$$\boldsymbol{f} = \boldsymbol{\kappa}\left(e^{\boldsymbol{\Phi}^{\boldsymbol{f}}} - e^{\boldsymbol{\Phi}^{\boldsymbol{r}}}\right) \tag{2.15}$$

$$\text{where } \boldsymbol{\kappa} = \frac{1}{f_0}\kappa \tag{2.16}$$

An alternative set of units uses the Faraday constant $F \approx 96.49\ (\mathrm{kC\,mol^{-1}})$ to replace chemical potential $\mu\ (\mathrm{J\,mol^{-1}})$ by $\phi = \frac{1}{F}\mu\ (\mathrm{V})$ and molar flow $v\ (\mathrm{mol\,s^{-1}})$ by $f = Fv\ (\mathrm{A})$ [28, 58]. In this case the normalised variables can be re-expressed as:

$$\boldsymbol{\phi} = \frac{\phi}{\phi_0} \tag{2.17}$$

$$\text{where } \phi_0 = \frac{1}{F}\mu_0 \approx 26.73\ (\mathrm{mV}) \tag{2.18}$$

$$\boldsymbol{f} = \frac{f}{f_0} \tag{2.19}$$

$$\text{where } f_0 = Fv_0 \approx 37.42\ (\mathrm{mA}) \tag{2.20}$$

$$\text{and } \boldsymbol{x} = \frac{Q}{x_0} \tag{2.21}$$

where $x_0\ (\mathrm{C})$ is the amount expressed in Coulombs.

2.3 Stoichiometry

As discussed previously [28, 40, 45] the stoichiometric representation of a biochemical system can be derived directly from the bond graph. In normalised form, the stoichiometric representation is:

$$\dot{\boldsymbol{x}} = N\boldsymbol{f} \tag{2.22}$$

$$\boldsymbol{\Phi}^{\boldsymbol{f}} = N^{f^T}\boldsymbol{\phi} \tag{2.23}$$

$$\boldsymbol{\Phi}^{\boldsymbol{r}} = N^{r^T}\boldsymbol{\phi} \tag{2.24}$$

$$\text{where } N = -N^f + N^r \tag{2.25}$$

$$\text{and } \dot{\boldsymbol{x}} = \frac{d\boldsymbol{x}}{d\boldsymbol{t}} \tag{2.26}$$

In the context of the example of § 2.1:

$$N^f = \begin{pmatrix} 1 & 0 \\ 0 & 1 \\ 0 & 0 \end{pmatrix} \qquad N^r = \begin{pmatrix} 0 & 0 \\ 1 & 0 \\ 0 & 1 \end{pmatrix} \qquad N = \begin{pmatrix} -1 & 0 \\ 1 & -1 \\ 0 & 1 \end{pmatrix} \tag{2.27}$$

where

$$\boldsymbol{\Phi} = \begin{pmatrix} \boldsymbol{\Phi}_A \\ \boldsymbol{\Phi}_B \\ \boldsymbol{\Phi}_C \end{pmatrix} \qquad \boldsymbol{x} = \begin{pmatrix} \boldsymbol{x}_A \\ \boldsymbol{x}_B \\ \boldsymbol{x}_C \end{pmatrix} \qquad \boldsymbol{f} = \begin{pmatrix} \boldsymbol{f}_1 \\ \boldsymbol{f}_2 \end{pmatrix} \tag{2.28}$$

As discussed on § 2.1, an open system can be obtained from a closed system by replacing dynamic **Ce** components by *chemostats*. In stoichiometric terms, Equation (2.22) is replaced by

$$\dot{\boldsymbol{x}} = N^c \boldsymbol{f} \tag{2.29}$$

where the chemodynamic stoichiometric matrix N^c is identical to the stoichiometric matrix N except that rows corresponding to chemostats are set to zero [28, 41].

In the context of the example of § 2.1, choosing both **Ce**:A and **Ce**:C to be chemostats gives:

$$N^c = \begin{pmatrix} 0 & 0 \\ 1 & -1 \\ 0 & 0 \end{pmatrix} \tag{2.30}$$

2.4 Linearisation

Linearisation in the context of bond graph models of engineering systems is discussed by Karnopp [59], who showed that the linearised system could also be represented as a bond graph. Linearisation in the context of bond graph models of biochemical systems is presented by Gawthrop and Crampin [41]. A key feature of biochemical systems is the presence of *conserved moieties* which lead to constraints on system states [40, § 3(b)] which in turn leads to reduced-order dynamical equations [40, § 3(c)]. If such state constraints are not explicitly accounted for, linearisation leads to systems with uncontrollable or unobservable states [60, 61] which appear as cancelling pole/zero pairs in the corresponding transfer functions. This paper uses the approach of Gawthrop and Crampin [41, § 4.2] to avoid this issue.

In particular, the linearised system is given in standard state-space form as:

$$\dot{\tilde{x}} = a\tilde{x} + b\tilde{u} \tag{2.31}$$

$$\tilde{y} = c\tilde{x} + d\tilde{u} \tag{2.32}$$

$$\text{where } \tilde{x} = x - \bar{x} \tag{2.33}$$

$$\tilde{y} = y - \bar{y} \tag{2.34}$$

$$\tilde{u} = u - \bar{u} \tag{2.35}$$

$\tilde{x}$, $\tilde{y}$ and $\tilde{u}$ are the deviation of the state x, the output y and the input u from the steady state values $\bar{x}$, $\bar{y}$ and $\bar{u}$ and a, b, c and d are matrices.

This linear system has the corresponding transfer function matrix $G(s)$ given in terms of the Laplace variable s as:

$$G(s) = c\left[sI - a\right]^{-1} b + d \tag{2.36}$$

where I is the $n_x \times n_x$ unit matrix. It is a standard result that the step response of the linear system represented by Equations (2.31) and (2.32) of Equation (2.36) is:

$$\tilde{y}(t) = g(t)\tilde{u} \tag{2.37}$$

Where the i, j element of the $n_y \times n_u$ matrix $g(t)$ is the unit step response of the ith element $\tilde{y}_i$ of the output vector $\tilde{y}$ when the jth element $\tilde{u}_j$ of $\tilde{u}$ is changed from 0 to 1 at time $t = 0$. Moreover, the time and Laplace domains are linked by:

$$g_\infty = \lim_{t\to\infty} g(t) = G(0) \tag{2.38}$$

$$g_0 = g(0) = \lim_{s\to\infty} G(s) \tag{2.39}$$

Equation (2.38) gives a convenient method for computing steady-state values from the transfer function and Equation (2.39) gives a convenient method for computing the initial response of the linearised system.

Although the actual sensitivity system response may be complicated, it is useful to provide an indicator τ of the overall time scale. In the case where $g_0 \neq 0$, the response is instantaneous and hence $\tau = 0$. When $g_0 = 0$, a first-order transfer function is of the form:

$$\frac{g_\infty}{1 + s\tau_0} \tag{2.40}$$

where τ_0 is the system time constant. In this case it is convenient to use $\tau = \tau_0$. In the general case, there are many possible time constants to choose. Here, we use *balanced order reduction* [62] to reduce the system order to unity select the corresponding time constant as in the first order case.

The three numbers g_0, g_∞ and τ provide a convenient summary of the dynamic properties of the linearised system (2.31) – (2.32). In the control literature, g_∞ is called the *DC gain* or *steady-state* gain of the linearised system (2.31) – (2.32).

3 The Sensitivity System

This section shows how the bond graph corresponding to the sensitivity system can be derived from the bond graph of the biochemical system itself. There are two approaches considered. § 3.1 shows how system components with variable parameters can be replaced by a sensitivity component represented itself by a bond graph thus giving an explicit bond graph for the sensitivity system. An alternative explored in § 3.2 is to derive the stoichiometric matrix of the bond graph biochemical system model, augment this matrix to give the stoichiometric matrix of the sensitivity system and then construct the corresponding bond graph. These conversions from stoichiometric matrix to bond graph and from bond graph to stoichiometric matrix are based on earlier work [45].

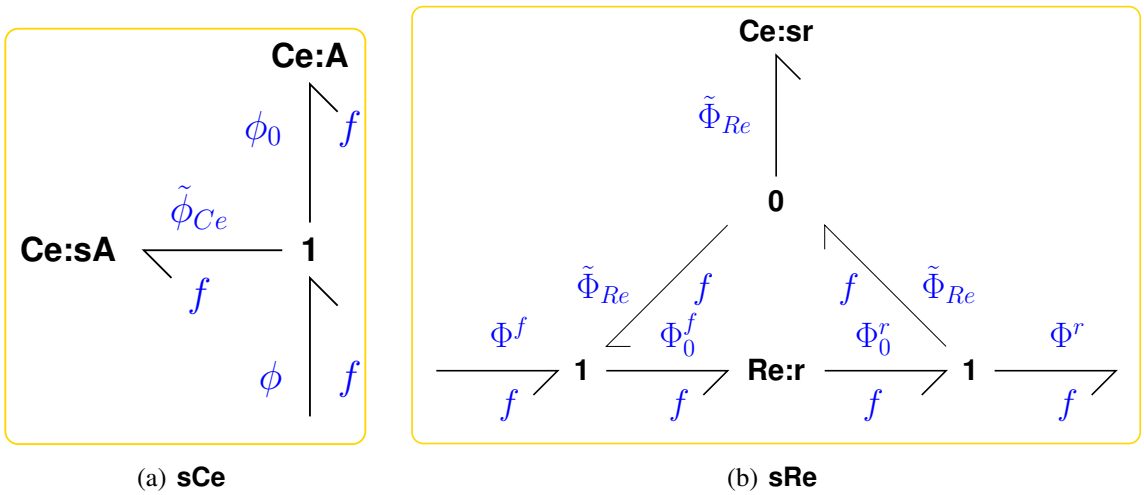

(a) **sCe** (b) **sRe**

Figure 2: Sensitivity components (a) **sCe** , the sensitivity **Ce** component, comprises the original **Ce** component **Ce**:A with normalised potential ϕ_0 and an additional chemostat **Ce**:sA with normalised potential $\tilde{\phi}_{\mathbf{Ce}}$ connected by a **1** junction so that the overall normalised potential is $\phi = \phi_0 + \tilde{\phi}_{\mathbf{Ce}}$. (b) **sRe** , the sensitivity **Re** component, comprises the original **Re** component **Re**:r with normalised forward and reverse potentials ϕ_0^f and ϕ_0^r and an additional chemostat **Ce**:sr with normalised potential $\tilde{\phi}_{\mathbf{Re}}$ connected by **1** junctions so that the overall normalised forward and reverse potentials are $\phi^f = \phi_0^f + \tilde{\phi}_{\mathbf{Re}}$ and $\phi^r = \phi_0^r + \tilde{\phi}_{\mathbf{Re}}$.

3.1 The sensitivity bond graph

The key idea in this paper is to replace each *parametric perturbation* by an *equivalent chemostat* (§ 2.1) and thus each bond graph component by a corresponding sensitivity bond graph component. This leads to:

1. a (nonlinear) sensitivity system represented by a bond graph for any biochemical system represented by a bond graph;
2. a (linear) local sensitivity system via linearisation [41] of the sensitivity system and
3. a stoichiometric interpretation of the sensitivity system.

3.1.1 The Ce sensitivity component

The constitutive relation (2.13) of the normalised **Ce** component has a single parameter $\boldsymbol{K}$. For a given substance, $\boldsymbol{K}$ is dependent on temperature.

The perturbation in this parameter is modelled using the multiplicative variable λ so that the constitutive relation (2.13) is replaced by:

$$\phi = \ln \lambda \boldsymbol{K} x = \ln \lambda + \ln \boldsymbol{K} x \tag{3.1}$$

Thus the effect of λ can be thought of as adding a second chemostat **Ce** component in such a way that the normalised potential $\tilde{\phi}_{\textbf{Ce}}$ adds to the normalised potential ϕ_0 of the original component to give

$$\boldsymbol{\phi} = \boldsymbol{\phi_0} + \tilde{\boldsymbol{\phi}}_{\textbf{Ce}} \tag{3.2}$$

$$\text{where } \tilde{\boldsymbol{\phi}}_{\textbf{Ce}} = \ln \lambda \tag{3.3}$$

Figure 2(a) gives the bond graph interpretation.

3.1.2 The chemostat sensitivity component

In bond graph terms, *chemostats* are **Ce** components with a fixed state $\boldsymbol{x} = \boldsymbol{x}_0$. As discussed in § 2.1 they represent substances such as metabolites which are external to the system. In biochemical terms, $\boldsymbol{x}_0$ can vary if the amount of the external substance changes. In this case, the fixed state x_0 can also be perturbed using the multiplicative parameter λ:

$$\boldsymbol{\phi} = \ln \boldsymbol{K} \lambda x_0 = \ln \lambda + \ln \boldsymbol{K} x_0 \tag{3.4}$$

Comparing Equation (3.4) with equation (3.1) it follows that a perturbation in the chemostat state x_0 can be modelled in the same way as a perturbation in $\boldsymbol{K}$.

3.1.3 The Re sensitivity component

The constitutive relation (2.15) of the normalised **Re** component has a single parameter $\boldsymbol{\kappa}$. In biochemical terms, $\boldsymbol{\kappa}$ can vary due to the amount of enzyme and the effect of enzyme inhibitors. The perturbation in the parameter $\boldsymbol{\kappa}$ is modelled using the multiplicative variable λ so that the constitutive relation (2.15) is replaced by:

$$\boldsymbol{f} = \lambda \boldsymbol{\kappa} \left(e^{\boldsymbol{\Phi}^{\boldsymbol{f}}} - e^{\boldsymbol{\Phi}^{\boldsymbol{r}}} \right) \tag{3.5}$$

$$= \boldsymbol{\kappa} \left(e^{\ln \lambda + \boldsymbol{\Phi}^{\boldsymbol{f}}} - e^{\ln \lambda + \boldsymbol{\Phi}^{\boldsymbol{r}}} \right) \tag{3.6}$$

Thus the effect of λ can be thought of as adding a chemostat **Ce** component in such a way that the normalised potential $\tilde{\phi}_{\textbf{Re}}$ adds to the normalised forward and reverse reaction potentials $\boldsymbol{\Phi}_{\boldsymbol{0}}^{\boldsymbol{f}}$ and $\boldsymbol{\Phi}_{\boldsymbol{0}}^{\boldsymbol{r}}$ of the original component to give

$$\boldsymbol{\Phi}^{\boldsymbol{f}} = \boldsymbol{\Phi}_{\boldsymbol{0}}^{\boldsymbol{f}} + \tilde{\boldsymbol{\phi}}_{\textbf{Re}} \tag{3.7}$$

$$\boldsymbol{\Phi}^{\boldsymbol{r}} = \boldsymbol{\Phi}_{\boldsymbol{0}}^{\boldsymbol{r}} + \tilde{\boldsymbol{\phi}}_{\textbf{Re}} \tag{3.8}$$

$$\text{where } \tilde{\boldsymbol{\Phi}}_{\textbf{Re}} = \ln \lambda \tag{3.9}$$

Figure 2(b) gives the bond graph interpretation.

Thus, for both the **Ce** and **Re** components, the perturbation λ is modelled as an additional chemostat with normalised potential $\tilde{\phi} = \ln \lambda$.

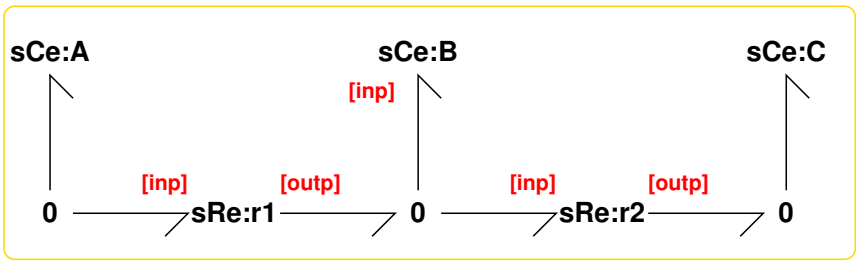

Figure 3: Sensitivity Example A $\rightleftharpoons$ B $\rightleftharpoons$ C. This figure is similar to Figure 1 except that the **Ce** and **Re** components have been replaced by the **sCe** and **sRe** components of Figure 2. As discussed in § 2.1, the system is open and **Ce**:A and **Ce**:C are chemostats; the corresponding sensitivity components are modelled in § 3.1.2.

3.1.4 Example A $\rightleftharpoons$ B $\rightleftharpoons$ C

The sensitivity system of Figure 3 gives the normalised flows $\boldsymbol{f}_1$ and $\boldsymbol{f}_2$ through the reaction components **Re**:$\mathbf{r_1}$ and **Re**:$\mathbf{r_2}$ as:

$$\boldsymbol{f}_1 = \lambda_1 \boldsymbol{\kappa}_1 \left(\lambda_A \boldsymbol{K}_A \boldsymbol{x}_A - \lambda_B \boldsymbol{K}_B \boldsymbol{x}_B\right) \tag{3.10}$$

$$\boldsymbol{f}_2 = \lambda_2 \boldsymbol{\kappa}_2 \left(\lambda_B \boldsymbol{K}_B \boldsymbol{x}_B - \lambda_C \boldsymbol{K}_C \boldsymbol{x}_C\right) \tag{3.11}$$

Note that if each $\lambda = 1$, the two flows correspond to the nominal system. The steady state flows correspond to $\dot{x}_B = 0$; that is $\boldsymbol{f}_1 = \boldsymbol{f}_2$ and thus:

$$\dot{\boldsymbol{x}}_B = \boldsymbol{f}_1 - \boldsymbol{f}_2 = -\left(\lambda_1 \boldsymbol{\kappa}_1 + \lambda_2 \boldsymbol{\kappa}_2\right) \lambda_B \boldsymbol{K}_B \boldsymbol{x}_B + \lambda_1 \boldsymbol{\kappa}_1 \lambda_A \boldsymbol{K}_A \boldsymbol{x}_A + \lambda_2 \boldsymbol{\kappa}_2 \lambda_C \boldsymbol{K}_C \boldsymbol{x}_C = 0 \tag{3.12}$$

The steady-state value $\bar{\boldsymbol{x}}_B$ of $\boldsymbol{x}_B$ is then given by:

$$\bar{\boldsymbol{x}}_B = \frac{\lambda_1 \boldsymbol{\kappa}_1 \lambda_A \boldsymbol{K}_A \boldsymbol{x}_A + \lambda_2 \boldsymbol{\kappa}_2 \lambda_C \boldsymbol{K}_C \boldsymbol{x}_C}{\lambda_B \boldsymbol{K}_B \left(\lambda_1 \boldsymbol{\kappa}_1 + \lambda_2 \boldsymbol{\kappa}_2\right)} \tag{3.13}$$

Again, the nominal steady state is obtained by setting each $\lambda = 1$.

3.2 A stoichiometric interpretation

The bond graph interpretation of the sensitivity system given in § 3.1 is conceptually useful and also provides a method for computer generation of the sensitivity system equations. This section presents an alternative approach to generating the sensitivity system equations from the bond graph using the stoichiometric representation outlined in § 2.3. For simplicity, the equations are generated for the sensitivity of every component.

The stoichiometry of the bond graph was considered in § 2.3. As discussed in § 3.1, the sensitivity bond graph consists of the original bond graph with extra **Ce** components acting as chemostats connected to the original **Ce** and **Re** components as indicated in Figure 2. These connections, together with those of the original bond graph, define the stoichiometry of the sensitivity bond graph. Following § 2.3, the equations for the closed sensitivity system where all

chemostats are regarded as ordinary **Ce** components is considered first. Assuming that a sensitivity component is appended for every **Ce** component and every **Re** component, the sensitivity system state $\boldsymbol{x}_s$ can be written as:

$$\boldsymbol{x}_s = \begin{pmatrix} \boldsymbol{x} \\ \tilde{\boldsymbol{x}}_{\textbf{Ce}} \\ \tilde{\boldsymbol{x}}_{\textbf{Re}} \end{pmatrix} \tag{3.14}$$

where $\boldsymbol{x}$ is the original system state and $\tilde{\boldsymbol{x}}_{\textbf{Ce}}$ and $\tilde{\boldsymbol{x}}_{\textbf{Re}}$ are the the states of the additional sensitivity **Ce** components associated with each **Ce** and **Re** components respectively.

Noting from Figure 2(a) that the sensitivity components associated with the **Ce** components share the same flows as the **Ce** components themselves, it follows from Equation (2.29) that, in the case of a closed system:

$$\dot{\tilde{\boldsymbol{x}}}_{\textbf{Ce}} = \dot{\boldsymbol{x}} = -N^f \boldsymbol{f^f} + N^r \boldsymbol{f^r} = N\boldsymbol{f} \tag{3.15}$$

Further, noting from Figure 2(b) that the sensitivity components associated with the **Ce** components share the same forward ($\boldsymbol{f^f}$) and reverse ($\boldsymbol{f^r}$) flows as the **Re** components themselves, it follows that:

$$\dot{\tilde{\boldsymbol{x}}}_{\textbf{Re}} = -\boldsymbol{f^f} + \boldsymbol{f^r} = 0 \tag{3.16}$$

From § 2.3, it follows that the stoichiometry of the sensitivity system corresponding to the open system with $\tilde{\boldsymbol{x}}_{\textbf{Ce}}$ and $\tilde{\boldsymbol{x}}_{\textbf{Re}}$ as chemostats is given in terms of the stoichiometry (Equations 2.29 – 2.24) by:

$$N_s^f = \begin{pmatrix} N^f \\ N^f \\ I \end{pmatrix} \qquad N_s^r = \begin{pmatrix} N^r \\ N^r \\ I \end{pmatrix} \qquad N_s = -N_s^f + N_s^r = \begin{pmatrix} N \\ N \\ 0 \end{pmatrix} \qquad N_s^c = \begin{pmatrix} N^c \\ 0 \\ 0 \end{pmatrix} \tag{3.17}$$

and

$$\dot{\boldsymbol{x}}_s = N_s^c \boldsymbol{f} \tag{3.18}$$

$$\boldsymbol{\Phi_s^f} = N_s^{f^T} \boldsymbol{\phi_s} \tag{3.19}$$

$$\boldsymbol{\Phi_s^r} = N_s^{r^T} \boldsymbol{\phi_s} \tag{3.20}$$

4 Linearisation of the Sensitivity System

§ 3 showed how the bond graph of the sensitivity system can be derived from the bond graph of the system itself; in general, this sensitivity system is nonlinear. A feature of the sensitivity system is that each *parameter variation* is replaced by a *chemostat* representing a system *input*. As discussed in § 2.4, nonlinear biochemical systems can be linearised. In the case of the non-linear sensitivity system of § 3 the inputs are the parameter variables λ (represented by chemostats) and

system flows were chosen to be the outputs. Hence the sensitivity system can be linearised about a steady-state to give a linear system of the form:

$$\dot{\tilde{\boldsymbol{x}}} = a\tilde{\boldsymbol{x}} + b\tilde{\Lambda} \tag{4.1}$$

$$\tilde{\boldsymbol{f}} = c\tilde{\boldsymbol{x}} + d\tilde{\Lambda} \tag{4.2}$$

where the column vector $\tilde{\Lambda}$ contains all of the sensitivity deviation variables $\tilde{\lambda}$. Comparison with Equations (2.31) and (2.32) shows that $\tilde{\Lambda}$ has the same role as the system input, and $\tilde{\boldsymbol{f}}$ the same role as the system output, in the linearised system.

As discussed in § 2.4, the three numbers g_0, g_∞ and τ provide a convenient summary of the dynamic properties of the linearised sensitivity system (4.1) – (4.2). In particular, g_∞ is the *DC gain* or *steady-state* gain of the linearised sensitivity system (4.1) – (4.2) and g_0 and τ represent the initial response and time-scale respectively.

Using the result of Karnopp [59] noted in § 2.4, it follows that the linearised sensitivity system also has a bond graph representation but with linear components.

4.1 Example A $\rightleftharpoons$ B $\rightleftharpoons$ C

As an illustrative example, this section continues the example of § 2.1 for the particular set of parameters:

$$\boldsymbol{K}_A = \boldsymbol{K}_B = \boldsymbol{K}_C = 1,\ \boldsymbol{\kappa}_1 = 1,\ \boldsymbol{\kappa}_2 = 9 \tag{4.3}$$

$$\boldsymbol{x}_A(0) = 2,\ \boldsymbol{x}_B(0) = \boldsymbol{x}_C(0) = 1 \tag{4.4}$$

In this special case, equation (3.13) becomes:

$$\bar{\boldsymbol{x}}_B = \frac{2\lambda_1\lambda_A + 9\lambda_2\lambda_C}{\lambda_B\left(\lambda_1 + 9\lambda_2\right)} \tag{4.5}$$

When all parameters are at their nominal values so that each $\lambda = 1$:

$$\bar{\boldsymbol{x}}_B = \frac{2+9}{1+9} = 1.1 \tag{4.6}$$

Similarly in the special case, the steady state values of $\boldsymbol{f}_1$ and $\boldsymbol{f}_2$ are

$$\bar{\boldsymbol{f}}_1 = \lambda_1\left(2\lambda_A - \lambda_B\bar{\boldsymbol{x}}_B\right) \tag{4.7}$$

$$\bar{\boldsymbol{f}}_2 = 9\lambda_2\left(\lambda_B\bar{\boldsymbol{x}}_B - \lambda_c\right) \tag{4.8}$$

and when all parameters are at their nominal values:

$$\bar{\boldsymbol{f}}_1 = \left(2 - \bar{\boldsymbol{x}}_B\right) = 0.9 \tag{4.9}$$

$$\bar{\boldsymbol{f}}_2 = 9\left(\bar{\boldsymbol{x}}_B - 1\right) = 0.9 \tag{4.10}$$

The steady-state sensitivities can be computed from Equations (4.5) – (4.8) by taking derivatives and substituting unit values for the remaining λ; for example:

$$\frac{\partial \bar{\boldsymbol{x}}_B}{\partial \lambda_A} = \frac{2\lambda_1}{\lambda_B\left(\lambda_1 + 9\lambda_2\right)} = \frac{2}{10} = 0.2 \tag{4.11}$$

$$\frac{\partial \bar{\boldsymbol{x}}_B}{\partial \lambda_1} = \frac{2\lambda_A\left(\lambda_B\left(\lambda_1 + 9\lambda_2\right)\right) - \lambda_B\left(2\lambda_1\lambda_A + 9\lambda_2\lambda_C\right)}{\left(\lambda_B\left(\lambda_1 + 9\lambda_2\right)\right)^2} = \frac{2 \times 10 - 1 \times 11}{10^2} = 0.09 \tag{4.12}$$

$$\frac{\partial \bar{\boldsymbol{f}}_1}{\partial \lambda_1} = \left(2\lambda_A - \lambda_B \bar{\boldsymbol{x}}_B\right) - \lambda_1\lambda_B \frac{\partial \bar{\boldsymbol{x}}_B}{\partial \lambda_1} = 0.9 - 0.09 = 0.81 \tag{4.13}$$

The dynamic linearisation of § 2.4 gives the transfer function:

$$\tilde{\boldsymbol{f}}_s(s) = G(s)\tilde{\Lambda}_s(s) \tag{4.14}$$

$$\text{where } \bar{\boldsymbol{f}} = \begin{pmatrix} \bar{\boldsymbol{f}}_1 & \bar{\boldsymbol{f}}_2 \end{pmatrix}^T \tag{4.15}$$

$$\bar{\Lambda} = \begin{pmatrix} \tilde{\lambda}_A & \tilde{\lambda}_B & \tilde{\lambda}_C & \tilde{\lambda}_1 & \tilde{\lambda}_2 \end{pmatrix}^T \tag{4.16}$$

where $\tilde{\boldsymbol{f}}_s(s)$ and $\tilde{\Lambda}_s(s)$ are the Laplace transforms the flows $\tilde{\boldsymbol{f}}$ and the sensitivity parameters $\tilde{\lambda}$ and $G(s)$ is the transfer function. In this case:

$$G(s) = \begin{pmatrix} \frac{2s+18}{s+10} & \frac{-1.1s}{s+10} & -9\frac{1}{s+10} & \frac{0.9s+8.1}{s+10} & 0.9\frac{1}{s+10} \\ \frac{18}{s+10} & \frac{9.9s}{s+10} & -9\frac{s+1}{s+10} & \frac{8.1}{s+10} & 0.9\frac{s+1}{s+10} \end{pmatrix} \tag{4.17}$$

Using Equation (2.38) of § 2.4 the steady-state gains relating the two flows to the five parameters are:

$$\bar{\boldsymbol{f}} = g_\infty \bar{\Lambda} \tag{4.18}$$

$$\text{where } g_\infty = G(0) \begin{pmatrix} 1.8 & 0. & -0.9 & 0.81 & 0.09 \\ 1.8 & 0. & -0.9 & 0.81 & 0.09 \end{pmatrix} \tag{4.19}$$

Using Equation (2.39) of § 2.4, the initial response is:

$$g_0 = g(0) = G(\infty) \begin{pmatrix} 2 & -1.1 & 0 & 0.9 & 0 \\ 0 & 9.9 & -9 & 0 & 0.9 \end{pmatrix} \tag{4.20}$$

The five figures 4(a)–4(e) correspond to the five columns of $g(t)$. In each case, the normalised response of the flow through **Re** r1 and **Re**:**r2** to a 10% step change in the corresponding parameter is shown as dashed lines and compared to the unit step response of the corresponding transfer function element of $G(s)$ together with the steady-stage gain g_∞. The initial and final values correspond to the elements of the matrices (4.20) and (4.19) respectively as indexed by (4.15) and (4.16).

The nonlinear response is close to that of the linearised response in each case. Figure 4(f) indicates how the discrepancy increases up to 1000% parameter variation.

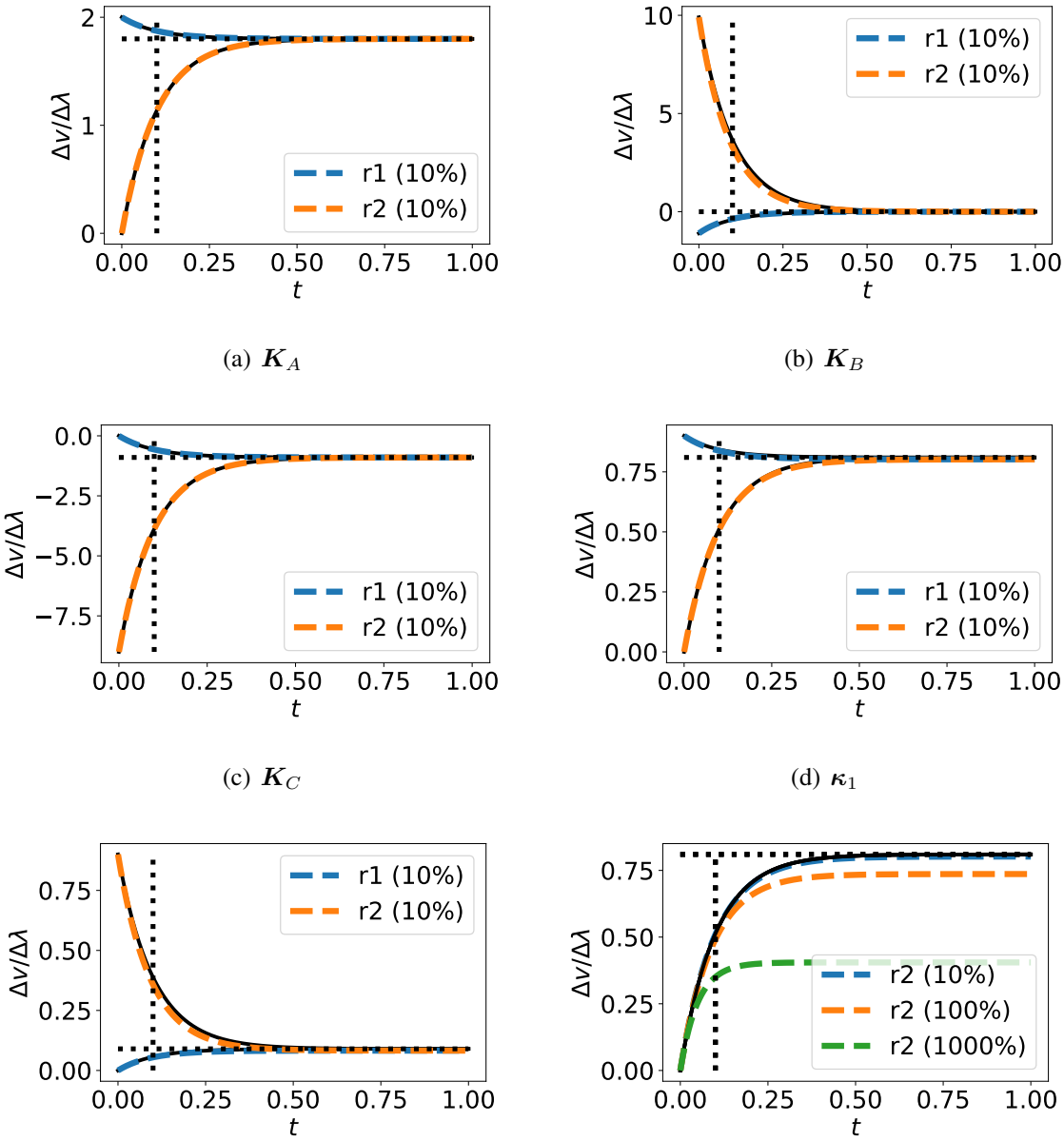

(a) $\boldsymbol{K}_A$ (b) $\boldsymbol{K}_B$ (c) $\boldsymbol{K}_C$ (d) $\boldsymbol{\kappa}_1$ (e) $\boldsymbol{\kappa}_2$ (f) λ

Figure 4: The sensitivity approximation. The normalised temporal responses of the flows through **Re** r1 and **Re**:**r2** to perturbations in (a) $\boldsymbol{K}_A$; (b) $\boldsymbol{K}_B$; (c) $\boldsymbol{K}_C$; (d) $\boldsymbol{\kappa}_1$; (e) $\boldsymbol{\kappa}_2$. Parameters are perturbed using a 10% step change. The black line is the linear sensitivity system response, the horizontal dashed black line the DC gain g_∞ and the vertical dashed black line the time-constant τ; the coloured dashed lines show the response of the simulated nonlinear system. (f) As (d) but the flow through **Re**:**r2** is shown for a 10%, 100% and 1000% change in parameter $\boldsymbol{\kappa}_1$.

5 Sloppy Parameter Sensitivities

In their seminal paper, Gutenkunst et al. [55] introduced the concept of *Sloppy Parameter Sensitivities* in the context of fitting parameters to experimental data. Following standard system identification practice [8], their method is based on a quadratic cost function of the variation of the the system time response as parameters vary. This gives rise to a data-dependent Hessian matrix; the eigenvalues and eigenvectors of this matrix determine parameter sensitivity.

This section looks at how this concept applies in the context of the linear time responses of the linearised sensitivity model of § 4. As an illustrative example, the sensitivity of internal flows through reactions and external flows associated with chemostats are considered here. In particular, define the quadratic function Q of normalised system flow variation $\tilde{\boldsymbol{f}}$:

$$Q = \frac{1}{t_f}\int_0^{t_f} \tilde{\boldsymbol{f}}^T \tilde{\boldsymbol{f}} dt \tag{5.1}$$

Using Equations (4.14),(2.37) it follows that the cost function Q may be rewritten explicitly in terms of the parameter variation vector $\tilde{\Lambda}$ as

$$Q = \tilde{\Lambda}^T H \tilde{\Lambda} \tag{5.2}$$

$$\text{where } H = \frac{1}{t_f}\int_0^{t_f} g(t)g(t)^T dt \tag{5.3}$$

The $n_\Lambda \times n_\Lambda$ matrix H is positive semi-definite and therefore has the eigenvalue decomposition:

$$H = \sum_{i=0}^{n_\Lambda} \sigma_i V_i V_i^T \tag{5.4}$$

where $\sigma_i \geq 0$ is the ith eigenvalue and the n_Λ column eigenvectors V_i are orthogonal and have unit length. Without loss of generality, assume that the eigenvectors are sorted with the largest first and the smallest last. The basic idea of sloppy parameter sensitivities [55] is that *small* eigenvalues σ_i correspond to directions (indicated by V_i) in parameter space where the effect of parameter variations is small – these parameter combinations are termed *sloppy*. Conversely, *large* eigenvalues σ_i correspond to directions where the effect of parameter variations is large – these parameter combinations are termed *stiff*.

In the special case that the final time t_f is large, H can be approximated in terms of the steady state time response g_∞ :

$$H \approx H_\infty = g_\infty g_\infty^T \tag{5.5}$$

In the special case of a single output, g_∞ is a vector and H_∞ has rank 1 and the matrix H_∞ has the decomposition

$$H_\infty = \sigma_1 V_1 V_1^T \tag{5.6}$$

$$\text{where } \sigma_1 = g_\infty^T g_\infty \tag{5.7}$$

$$\text{and } V_1 = \pm\frac{1}{\sqrt{\sigma_1}} g_\infty \tag{5.8}$$

thus $n_\Lambda - 1$ eigenvalues are zero. The corresponding cost function is defined as:

$$Q_\infty = \tilde{\Lambda}^T H_\infty \tilde{\Lambda} \tag{5.9}$$

5.1 The two-parameter case

Because Q is a quadratic function of the sensitivity parameter vector Λ each constant value of Q corresponds to an ellipsoid in n_λ-dimensional space. In particular, in two-dimensional parameter space, this eigen-decomposition gives elliptical contours of $Q = 1$ with minor axis corresponding to $1/\sqrt{\sigma_1}$ and major axis corresponding to $1/\sqrt{\sigma_2}$ where $\sigma_1 \geq \sigma_2$ – see Figure 1A of Gutenkunst et al. [55]. In the particular case of Equation (5.6), $\sigma_2 = 0$ the major axis has infinite length and the ellipse degenerates to two parallel lines. This two-parameter case is illustrated in Figure 5 for both $Q = 1$ and $Q_\infty = 1$.

5.2 Example A $\rightleftharpoons$ B $\rightleftharpoons$ C

Here, we consider the steady-state sensitivity of the biochemical pathway A $\rightleftharpoons$ B $\rightleftharpoons$ C. For simplicity, consider the particular case where only the two sensitivity parameters λ_{r1} and λ_{r2} (corresponding to **Re**:$\mathbf{r_1}$ and **Re**:$\mathbf{r_2}$) are varied and the flow through **Re**:$\mathbf{r_1}$ is measured. The case where only the two sensitivity parameters λ_A and λ_C (corresponding to **Ce**:A and **Ce**:B) are varied can be analysed in a similar fashion.

The eigenvalue σ_1 and eigenvector V_1 corresponding to H_∞ are given by:

$$\sqrt{\sigma}_1 = 0.81 \qquad V_1\Lambda = +0.994\lambda_{r1} + 0.110\lambda_{r2} \tag{5.10}$$

When $t_f = 1$, the two eigenvalues and eigenvectors of H are given by:

$$\sqrt{\sigma}_1 = 0.82 \qquad V_1\Lambda = +0.995\lambda_{r1} + 0.097\lambda_{r2} \tag{5.11}$$

$$\sqrt{\sigma}_2 = 0.021 \qquad V_2\Lambda = +0.995\lambda_{r2} - 0.097\lambda_{r1} \tag{5.12}$$

The ellipse corresponding to $Q = 1$ (5.2) appears in Figure 5(a) together with the two parallel lines corresponding to $Q_\infty = 1$ (5.9).

When $t_f = 1000$, the two eigenvalues and eigenvectors of H are given by:

$$\sqrt{\sigma}_1 = 0.82 \qquad V_1\Lambda = +0.995\lambda_{r1} + 0.097\lambda_{r2} \tag{5.13}$$

$$\sqrt{\sigma}_2 = 0.021 \qquad V_2\Lambda = +0.995\lambda_{r2} - 0.097\lambda_{r1} \tag{5.14}$$

In this case, the first eigenvalue and eigenvector of H are close to that of H_∞; and the second eigenvector $\sigma_2 \approx 0$. Thus, in this case, $H \approx H_\infty$. The ellipse corresponding to Q (5.2) appears in Figure 5(b) together with the two parallel lines corresponding to Q_∞ (5.9).

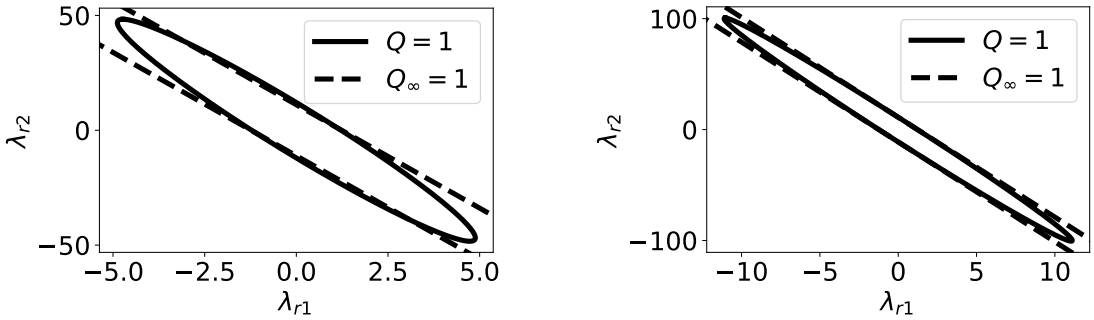

(a) Vary **Re** : $t_f = 1$

(b) Vary **Re** : $t_f = 1000$

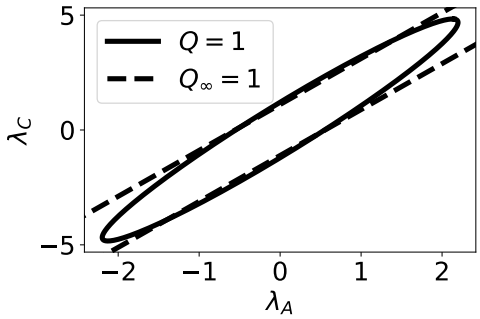

(c) Vary **Ce** : $t_f = 1$

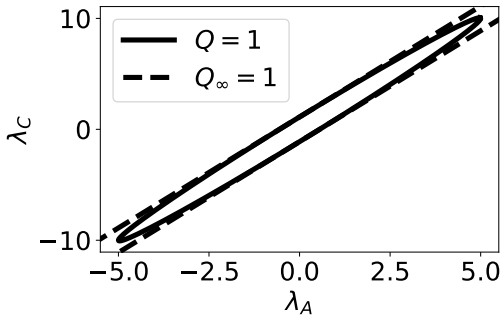

(d) Vary **Ce** : $t_f = 1000$

Figure 5: Sloppy parameters. As discussed in § 5.1, the contours of the two-parameter cost function corresponding to constant values $Q = 1$ are ellipses in parameter space whereas $Q_\infty = 1$ corresponds to two parallel lines. (a) The parameters λ_{r1} and λ_{r2}, corresponding to the two **Re** components, are varied. (b) As (a) but with a long timescale; as expected, $Q \approx Q_\infty$. (c) The parameters λ_A and λ_C , corresponding to the two chemostat **Ce** components, are varied. (d) As (c) but with a long timescale.

6 Example: Modulated Enzyme-catalysed reaction

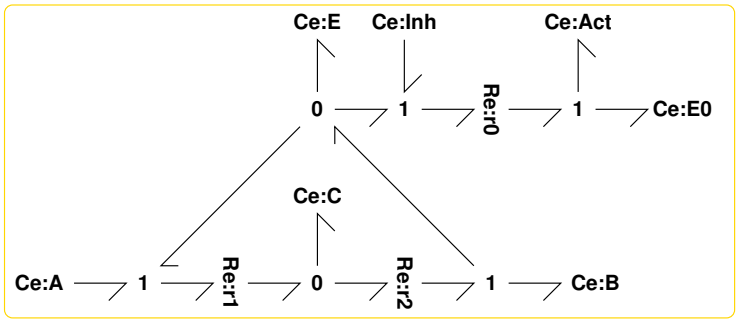

Figure 6: Modulated Enzyme-catalysed reaction: For the purposes of this example, all parameters are unity and all initial states are unity *except* the total enzyme amount $e_0 = \boldsymbol{x}_E + \boldsymbol{x}_C + \boldsymbol{x}_{E0} = 10$ and $\boldsymbol{x}_B = 10^{-3}$.

Enzyme-catalysed reactions are an important control mechanism in biochemical systems [63]. One such mechanism is an enzyme-catalysed reaction with competitive activation and inhibition; which has been analysed within the bond graph context [52] and is shown in Figure 6. This simple system is used to illustrate the sensitivity methods of this paper. In particular, the dynamic sensitivities are derived and compared with the steady-state gain g_∞ and time constant τ characterisation of the linear response. In addition, the variation of steady-state gain g_∞ with steady-state flows through **Re**:$\mathbf{r_1}$ and **Re**:$\mathbf{r_2}$ is investigated.

The four plots of Figure 7 show the dynamic sensitivity of the normalised flows in **Re**:$\mathbf{r_1}$ and **Re**:$\mathbf{r_2}$ to step changes in $\tilde{\lambda}_{X_A}$, $\tilde{\lambda}_{r_1}$, $\tilde{\lambda}_{X_{Act}}$ and $\tilde{\lambda}_{X_{Inh}}$. In the case of $\tilde{\lambda}_{X_A}$ and $\tilde{\lambda}_{r_1}$, the flow through **Re**:$\mathbf{r_1}$ changes instantaneously and that through **Re**:$\mathbf{r_2}$ has a steady-state gain of about $g_\infty = 1.60$ for $\tilde{\lambda}_{X_A}$ and $g_\infty = 0.80$ for $\tilde{\lambda}_{r_1}$. The normalised time constant is about $\tau = 0.32$ in each case. In the case of $\tilde{\lambda}_{X_{Act}}$ and $\tilde{\lambda}_{X_{Inh}}$, the flow through both **Re**:$\mathbf{r_1}$ and**Re**:$\mathbf{r_2}$ does not change instantly and has has a steady-state gain of about $g_\infty = \pm 0.8$ and time constant of about $\tau = 0.4$.

Because the dynamics of the enzyme-catalysed reaction with competitive activation and inhibition are non-linear, the linearised gains are a function of the operating point. Figure 8(a) shows how the steady-state flow $\bar{\boldsymbol{f}}_1 = \bar{\boldsymbol{f}}_2$ varies with the amount of substrate $\boldsymbol{x}_A$; this is the typical reversible Michaelis-Menten curve saturating at a value dependent on the total enzyme. The system steady-state state is computed for a range of flows and the corresponding linearised gains are plotted in Figures 8(b) – 8(d). At small flows, the steady-state gains g_∞ in Figures 8(b) – 8(d) are small because they correspond to flow sensitivity. At high flows, the flow is constrained by the maximum Michaelis-Menten flow $V_{max} = e_0 \kappa_2 K_c$ where e_0 is the total amount of bound and unbound enzyme; and so is independent of all of the sensitivity parameters shown except for κ_2. Hence $g_\infty = 0$ when the flow is saturated in all cases shown except for κ_2.

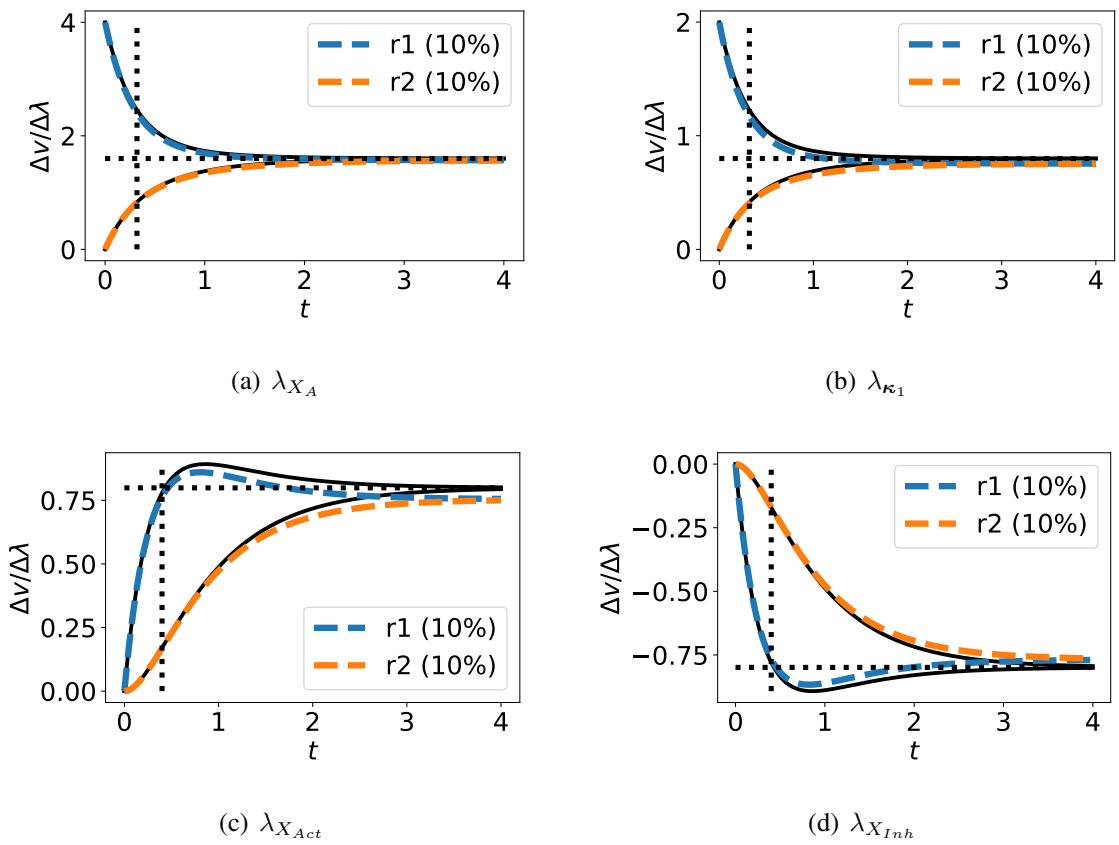

(a) λ_{X_A}

(b) λ_{κ_1}

(c) $\lambda_{X_{Act}}$

(d) $\lambda_{X_{Inh}}$

Figure 7: Enzyme-catalysed reaction: Dynamical Sensitivities. The normalised flows in the two reaction components **Re**:r1 **Re**:r2 are plotted against normalised time in response to a 10% change in the quantities indicated; the dashed coloured lines show the simulated response The firm black lines show the theoretical sensitivity result and the dashed back lines the steady-state sensitivity g_∞ and normalised time constant τ.

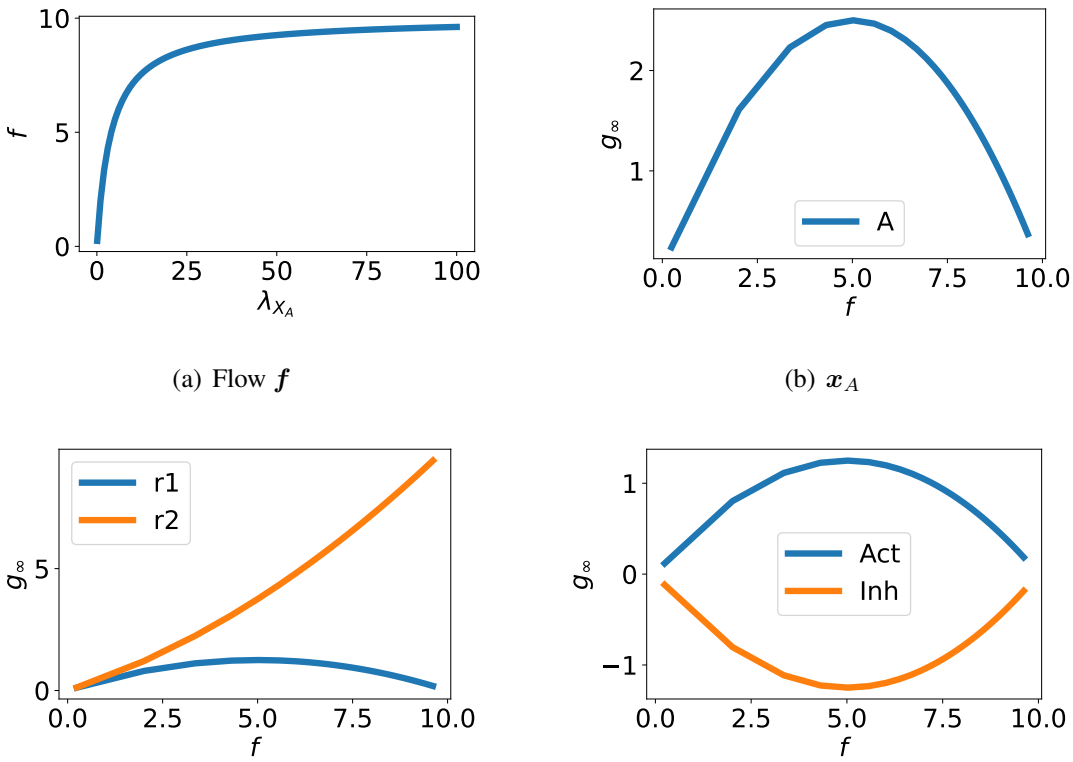

(a) Flow $\boldsymbol{f}$

(b) $\boldsymbol{x}_A$

(c) $\boldsymbol{\kappa}_1, \boldsymbol{\kappa}_2$

(d) $\boldsymbol{x}_{Act}, \boldsymbol{x}_{Inh}$

Figure 8: Enzyme-catalysed reaction: Variation of sensitivity with steady-state. (a) The steady-state flow $\boldsymbol{f} = \boldsymbol{f}_1 = \boldsymbol{f}_2$ is a non-linear function of the substrate concentration: the classical Michaelis-Menten curve. The corresponding steady-state values of the state of each **Ce** component is computed for a number of values of $\boldsymbol{f}$. (b) The sensitivity gain relating flow to $\boldsymbol{x}_A$ is plotted against the steady-state flow $\bar{\boldsymbol{f}}$. (c) As (b) but with parameters corresponding to **Re**:$\mathbf{r1}$ and **Re**:$\mathbf{r2}$. (c) As (b) but with parameters corresponding to **Ce**:$\mathbf{Act}$ and **Ce**:$\mathbf{Inh}$. As expected, activation increases, and inhibition decreases, steady-state flow; in both cases the modulation is most effective at flows corresponding to half the saturated flow.

7 Example: Pentose Phosphate Pathway

The Pentose Phosphate Pathway [64, 65] provides a number of different products from the metabolism of glucose. This flexibility is adopted by proliferating cells, such as those associated with cancer, to adapt to changing requirements of biomass and energy production [66, 67]. The *E. coli* Core Model [68, 69] is a well-documented and readily-available stoichiometric model of a biomolecular system. As discussed previously [45], species, reactions and stoichiometric matrix pertaining to the Pentose Phosphate Pathway were extracted, a bond graph model created and parameters fitted using experimental data from *E. coli* [70]; the normalising time $t_0 = 7.95\,\mathrm{s}$ [45]. This section examines the sensitivity properties of this model.

The sensitivity system was created using the approach of § 3.2 and linearised as discussed in § 2.4 and § 4. Figure 9 shows the steady-state gain g_∞ from Equation (2.38) for the flows of three products: R_5P, NADPH and G_3P for two cases: sensitivity with respect to reaction constants and sensitivity with respect to chemostat states. Figure 10 shows the time constant τ for each of the six cases of Figure 9 computed as discussed in § 2.4. The rate parameter associated with G_6PDH_2R has the most influence over R_5P and NADPH production (Figure 9(a,c)). These rates of production are also most sensitive to the concentrations of G_6P and NADP, and the concentration of R_5P has a substantial effect on its own rate of production (Figure 9(b,d)). Different reactions and species are involved in the regulation of G_3P production, with PGI and PFK being the primary reactions (Figure 9(e)); and G_6P and ATP being the primary metabolites (Figure 9(f)).

7.1 Parameter sensitivity

The linearised sensitivity system (§ 4) is an approximation to the nonlinear sensitivity system (§ 3.1) for two reasons: it varies with the steady state of the non-linear system about which the linearisation is performed and the discrepancy between the linear and non linear system responses increases with the amplitude of the parameter variation. The former is discussed in § 6, Figure 8; the latter is examined further in this section in the context of the Pentose Phosphate Pathway example.

Figure 11 shows the effect of varying the amplitude of the sensitivity variable $\lambda_{G6PDH2R}$. Figure 11(a) gives the non-linear deviation of the flow $\Delta \boldsymbol{f}_{R5P}$ from its steady-state value normalised by the change in sensitivity variable $\Delta\lambda_{G6PDH2R}$ for three values of the sensitivity variable $\Delta\lambda_{G6PDH2R}$. As expected, the error increases with $\Delta\lambda_{G6PDH2R}$ but, in this case, a tenfold increase only gives a 20% error. Figure 11(b) gives a similar result for product NADPH and Figure 11(c) gives a similar result for substrate G_6P. Figure 11(d) summarises these results in terms of the steady-state linearisation error ϵ where:

$$\epsilon = \frac{g_N - g_\infty}{g_\infty} \tag{7.1}$$

$$\text{where } g_N = \frac{\Delta \boldsymbol{f}_\infty}{\Delta\lambda} \tag{7.2}$$

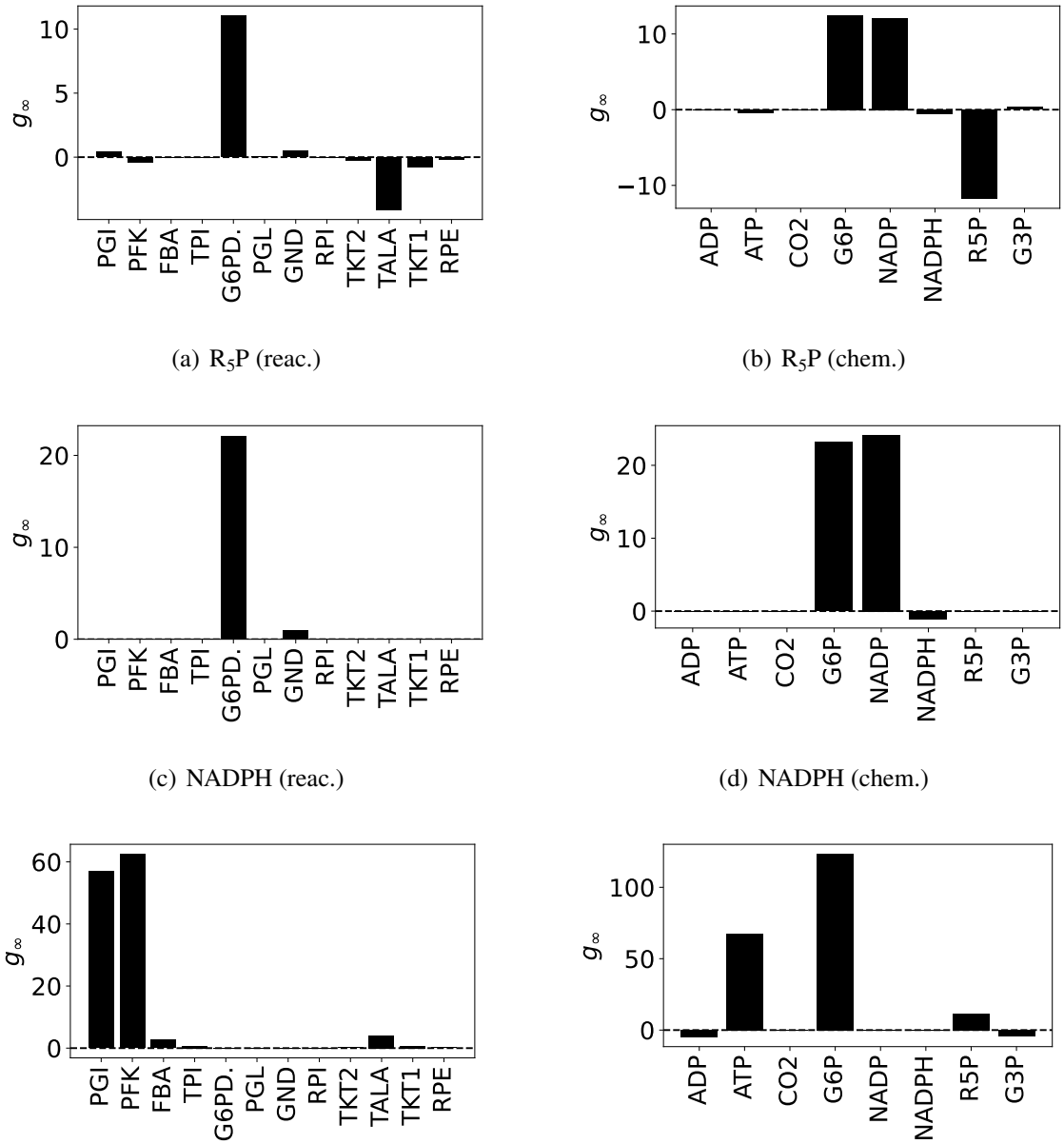

(a) R_5P (reac.)

(b) R_5P (chem.)

(c) NADPH (reac.)

(d) NADPH (chem.)

(e) G_3P (reac.)

(f) G_3P (chem.)

Figure 9: Pentose Phosphate Pathway: Steady-state sensitivity g_∞. (a) The steady-state sensitivity g_∞ of the flow of product R_5P with respect to the reaction sensitivity variables $\lambda_{\mathbf{Re}}$ are shown for all reactions in the network. The dominant reaction is G_6PDH_2R. (b) The steady-state sensitivity g_∞ of the flow of product R_5P with respect to chemostat sensitivity variables $\lambda_{\mathbf{Ce}}$. Flow is increased primarily by G_6P and NADP; flow is decreased primarily by R_5P. (c) As (a) but for product NADPH; again, the dominant reaction is G_6PDH_2R. (d) As (b) but for product NADPH. Again, flow is increased primarily by G_6P and NADP. (e) As (a) but for product G_3P; in this case, the dominant reactions are PGI and PFK. (f) As (b) but for product G_3P; in this case flow is increased primarily by G_6P and ATP.

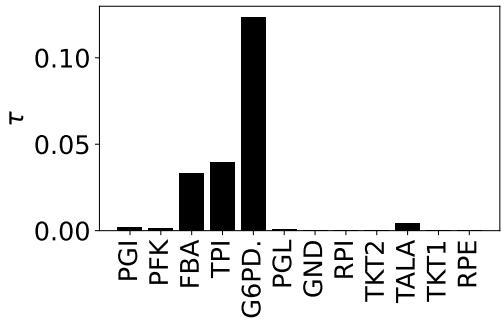

(a) R_5P (reac.)

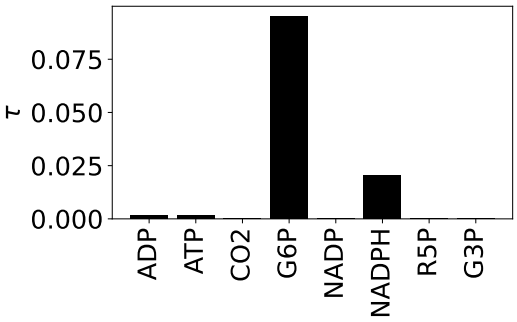

(b) R_5P (chem.)

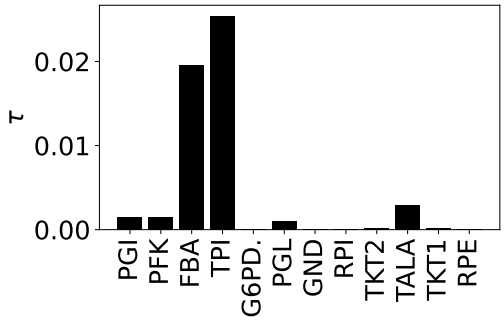

(c) NADPH (reac.)

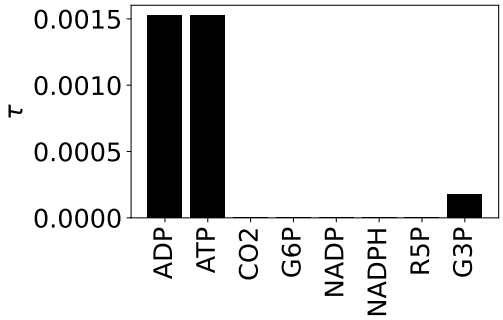

(d) NADPH (chem.)

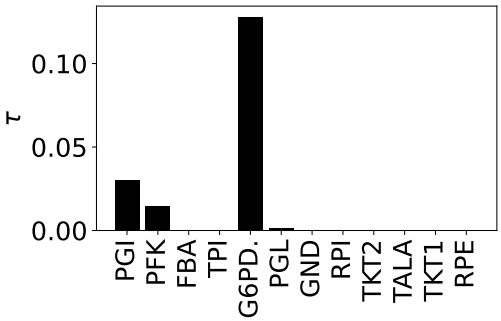

(e) G_3P (reac.)

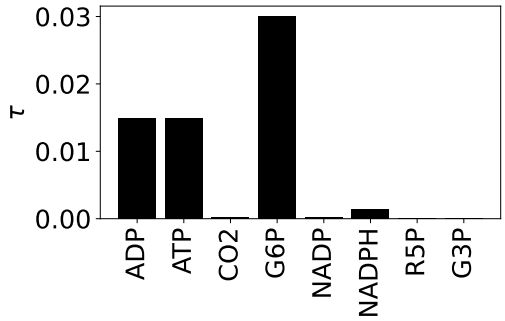

(f) G_3P (chem.)

Figure 10: Pentose Phosphate Pathway: Sensitivity normalised time constant τ. The normalising time $t_0 = 7.95\,\mathrm{s}$ [45]. (a) The Sensitivity time constants τ of the flow of product R_5P with respect to the reaction sensitivity variables $\lambda_{\mathbf{Re}}$ are shown for all reactions in the network. The sensitivity time constant for the dominant reaction G_6PDH_2R is about $\tau = 0.1$ – see Figure 11. (b) The Sensitivity time constant τ of the flow of product R_5P with respect to chemostat sensitivity variables $\lambda_{\mathbf{Ce}}$. The time constant for G_6P is greater than that for NADPH reflecting the greater number of intervening reactions. (c) As (a) but for product NADPH; the sensitivity to dominant reaction G_6PDH_2R has no delay ($\tau = 0$) as NADPH is a product of that reaction. (d) As (b) but for product NADPH. The sensitivity to dominant species G_6P has no delay ($\tau = 0$) as NADPH is a product of the same reaction. (e) As (a) but for product G_3P; the dominant reactions PGI and PFK have a relatively small τ due to their proximity to this product. (f) As (b) but for product G_3P; the dominant substrates G_6P and ATP have relatively small τ decreasing with proximity to the product.

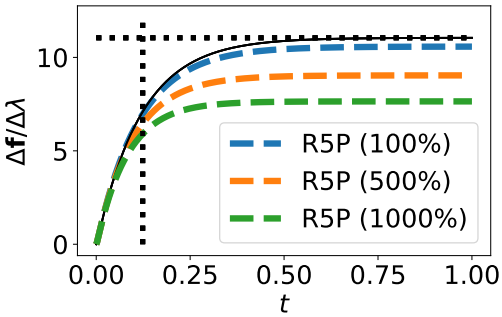

(a) G_6PDH_2R–R_5P

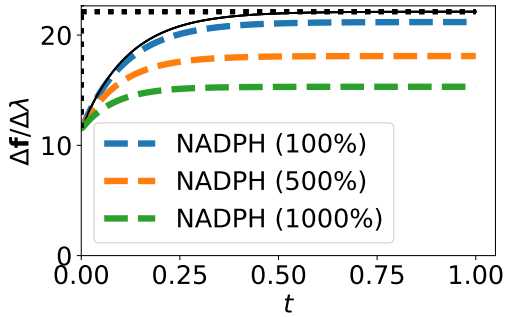

(b) G_6PDH_2R–NADPH

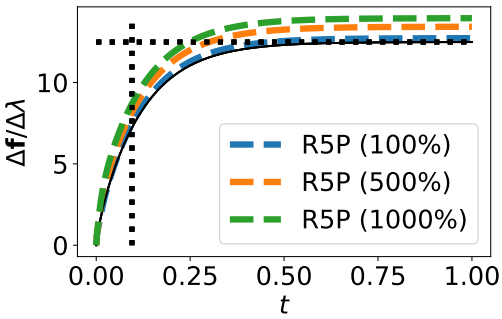

(c) G_6P–R_5P

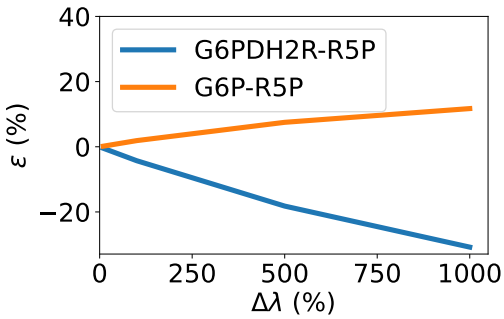

(d) Linearisation error

Figure 11: Sensitivity approximation. (a) The flow of product R_5P is shown for a 100%,500% and 1000% change in parameter $\lambda_{G6PDH2R}$. (b) As (a) but showing flow of product NADPH (c) As (a) but with change in the concentration of G_6P. (d) Linearisation error. $\epsilon = (g_N - g_\infty)/g_\infty$ where g_∞ is the steady-state (DC) gain of the linearised system, $g_N = \Delta\dot{\boldsymbol{x}}_{ss}/\Delta\lambda$ and $\dot{\boldsymbol{x}}_{ss}$ is the steady-state value of $\dot{\boldsymbol{x}}$. The gains are shown for three cases: sensitivity of R_5P with respect to G_6PDH_2R and G_6P.

7.2 Sloppy parameters

This section applies the methods of § 5 to the Pentose Phosphate Pathway model. In particular, the chemostat flows associated with product R_5P is examined. Because this is a high-order system, the eigenvalue/eigenvector approach can be utilised to simplify the results by discarding small eigenvalues and small components of eigenvectors. In this case eigenvalues less than 1% of the largest eigenvalue are discarded, and within each eigenvector, components less than 10% of the largest element are discarded. For illustration, the sensitivity of the flow of R_5P is investigated as all reaction constants are varied. In each case, the results using the Q_∞ cost function in Equation (5.9) are compared with those from Q (5.2) when the final time t_f is chosen by the `step_response` function of the Python Control Systems Library [71]).

The eigenvalue σ_1 and eigenvector V_1 corresponding to H_∞ are given by:

$$\sqrt{\sigma}_1 = 12 \qquad V_1\Lambda = +0.93\lambda_{G6PDH2R} - 0.35\lambda_{TALA} \tag{7.3}$$

When multiplied by $\sqrt{\sigma}$, the eigenvector elements correspond to the two largest values of g_∞ given in Figure 9(a).

The significant eigenvalues, and corresponding significant elements of the eigenvector corresponding to H are given by:

$$\sqrt{\sigma}_1 = 11 \qquad V_1\Lambda = +0.91\lambda_{G6PDH2R} - 0.38\lambda_{TALA} + 0.15\lambda_{GND} \tag{7.4}$$

$$\sqrt{\sigma}_2 = 3 \qquad V_2\Lambda = +0.94\lambda_{GND} - 0.25\lambda_{G6PDH2R} - 0.21\lambda_{TALA} \tag{7.5}$$

8 Conclusion

It has been shown that the sensitivity properties of the model of a biochemical system modelled using the bond graph formulation can be examined by creating a corresponding sensitivity bond graph model. The sensitivity model can be created by either replacing bond graph components with variable parameters by a corresponding sensitivity component or via a stoichiometric approach. Either approach can be used to automatically convert the original bond graph to a sensitivity bond graph. Within the sensitivity model, the parameter variation appears as a set of additional inputs modelled as bond graph chemostat components. Hence previously developed linearisation approaches can be used to linearise the nonlinear sensitivity system with respect to parameter variation to give local sensitivity results.

The well known "sloppy parameter" method, and its corresponding cost-functions have been incorporated into the sensitivity approach of this paper and lead to illuminated eigenvalue/eigenvector decomposition of a Hessian matrix associated with the local sensitivity results.

The results have been illustrated using a previously-derived model of the Pentose Phosphate Pathway. In this particular case, the linearised sensitivity system is compared to the nonlinear case and found to form an accurate approximation. As is well-known [64, 22.6], the reaction G_6PDH_2R is an important regulator of the Pentose Phosphate Pathway; the sensitivity analysis does indeed show that product flows depend strongly on this reaction.

The methods presented here could potentially be used to analyse omics data. While statistical and bioinformatics methods can reveal analytes of interest, conducting a sensitivity analysis on a mechanistic model can help researchers to assess the importance of potential changes in these analytes. Recent metabolomics and proteomics analysis of heart tissue [72] gives experimental evidence for how disease affects the heart in terms of its biochemistry. Combining this differential omics analysis with corresponding biochemical sensitivity models will allow us to map the omics data onto medically-significant physical phenomena such as cardiovascular disease. Parameters with high sensitivity may point towards potential targets for biomedical interventions.

A major challenge in systems biology is model parameterisation, particularly for large-scale models [73]. Sensitivity analysis can inform experimental design to reduce uncertainty in model predictions. Our results in § 7.1 indicate that not all parameters are equally important for the behaviour of a model, and that different parameters are important for describing different aspects of model behaviour. This observation has been mirrored in other sensitivity studies [55, 74]. Thus, determining the 'stiff' combinations of parameters can help to optimise for knowledge gained with limited experimental resources. Furthermore, analysing the time constants can be used to assess the biological relevance of parameter sets in machine learning approaches to parameterisation [75, 76]. Our approach builds on existing techniques by reframing parameters in a thermodynamically consistent context, which can in some cases reduce the number of parameters and better distinguish between the individual contributions of reactions and metabolites [77, 78].

There is a wealth of control-theoretic results applicable to linear systems. As indicated in the example of § 6, modulating the parameters of enzyme-catalysed reactions is a key strategy in human cellular control systems. The sensitivity models of this paper provide a foundation for applying such control-theoretic results to understand biochemical control systems. These methods are particularly relevant for attempts to rationally engineer pathways in synthetic biology, where sensitive parameters indicate potential targets of modification [79]. In many cases, biological networks are designed to be robust to noise, independent of parameter values [80, 81]. However, this robustness often comes at a cost to resource and energy consumption [41, 82], and in some cases, noise is harnessed for biological control [83, 84]. A bond graph modelling approach frames these behaviours in a thermodynamic context, allowing investigations into trade-offs between energy consumption and performance.

Author Contributions

PJG prepared the numerical results and drafted the manuscript; PJG and MP discussed the results and revised the manuscript. PJG and MP approved the final version for publication.

Acknowledgements

PJG would like to thank the Faculty of Engineering and Information Technology, University of Melbourne, for its support via a Professorial Fellowship. MP was supported by a Postdoctoral

Research Fellowship from the School of Mathematics and Statistics at the University of Melbourne.

Data Accessibility

The figures and tables in this paper were generated using the Jupyter notebooks and Python code available at `https://github.com/gawthrop/Sensitivity23`.

References

[1] C. Y. Huang and J. E. Ferrell. Ultrasensitivity in the mitogen-activated protein kinase cascade. *Proceedings of the National Academy of Sciences*, 93(19):10078–10083, Sep 1996. ISSN 0027-8424. doi:10.1073/pnas.93.19.10078.

[2] Paul M. Frank. *Introduction to System Sensitivity Theory*. Academic Press, New York, 1978.

[3] Mansour Eslami. *Theory of sensitivity in dynamic systems: an introduction*. Springer, Berlin, 1994. ISBN 978-3-662-01634-3.

[4] S. Skogestad and I Postlethwaite. *Multivariable Feedback Control Analysis and Design*. Wiley, New York, 1996.

[5] G.C. Goodwin, S.F. Graebe, and M.E. Salgado. *Control System Design*. Prentice Hall, Englewood Cliffs, New Jersey, 2001.

[6] D.J. Winning, E.H.T. El-Shirbeeny, E.C. Thompson, and D.J. Murray-Smith. Sensitivity method for online optimisation of a synchronous generator excitation controller. *Proceedings IEE Part D: Control Theory and Applications*, 124(7):631–638, July 1977.

[7] P. Eykhoff. *System Identification*. Wiley, 1974.

[8] Lennart Ljung. *System Identification: Theory for the User*. Information and Systems Science. Prentice-Hall, Englewood Cliffs, New Jersey, 2nd edition, 1999.

[9] Hiroaki Kitano. Computational systems biology. *Nature*, 420:206–210, November 2002. ISSN 0028-0836. doi:10.1038/nature01254.

[10] Hiroaki Kitano. Systems biology: A brief overview. *Science*, 295(5560):1662–1664, 2002. doi:10.1126/science.1069492.

[11] P. Kohl, E. J. Crampin, T. A. Quinn, and D. Noble. Systems biology: An approach. *Clin Pharmacol Ther*, 88:25–33, July 2010. ISSN 0009-9236. doi:10.1038/clpt.2010.92.

[12] Z. Zi. Sensitivity analysis approaches applied to systems biology models. *IET Systems Biology*, 5:336–346(10), November 2011. ISSN 1751-8849. doi:10.1049/iet-syb.2011.0015.

[13] Paolo Cazzaniga, Chiara Damiani, Daniela Besozzi, Riccardo Colombo, Marco S. Nobile, Daniela Gaglio, Dario Pescini, Sara Molinari, Giancarlo Mauri, Lilia Alberghina, and Marco Vanoni. Computational strategies for a system-level understanding of metabolism. *Metabolites*, 4(4):1034–1087, 2014. ISSN 2218-1989. doi:10.3390/metabo4041034.

[14] Thomas J Snowden, Piet H van der Graaf, and Marcus J Tindall. Methods of model reduction for large-scale biological systems: a survey of current methods and trends. *Bulletin of mathematical biology*, 79(7):1449–1486, 2017. doi:10.1007/s11538-017-0277-2.

[15] George Qian and Adam Mahdi. Sensitivity analysis methods in the biomedical sciences. *Mathematical Biosciences*, 323:108306, 2020. ISSN 0025-5564. doi:https://doi.org/10.1016/j.mbs.2020.108306.

[16] J.A. Burns, A. Cornish-Bowden, A.K. Groen, R. Heinrich, H. Kacser, J.W. Porteous, S.M. Rapoport, T.A. Rapoport, J.W. Stucki, J.M. Tager, R.J.A. Wanders, and H.V. Westerhoff. Control analysis of metabolic systems. *Trends in Biochemical Sciences*, 10(1):16 –, 1985. ISSN 0968-0004. doi:10.1016/0968-0004(85)90008-8.

[17] Athel Cornish-Bowden and María Luz Cárdenas, editors. *Control of metabolic processes*, volume 190. Springer Science & Business Media, 1989.

[18] David A Fell. Metabolic control analysis: a survey of its theoretical and experimental development. *Biochemical Journal*, 286(Pt 2):313–330, 1992.

[19] Reinhart Heinrich and Stefan Schuster. *The regulation of cellular systems*. Chapman & Hall New York, 1996.

[20] David Fell. *Understanding the control of metabolism*, volume 2 of *Frontiers in Metabolism*. Portland press, London, 1997. ISBN 1 85578 047 X.

[21] Brian P. Ingalls and Herbert M. Sauro. Sensitivity analysis of stoichiometric networks: an extension of metabolic control analysis to non-steady state trajectories. *Journal of Theoretical Biology*, 222(1):23 – 36, 2003. ISSN 0022-5193. doi:10.1016/S0022-5193(03)00011-0.

[22] Brian P. Ingalls. A frequency domain approach to sensitivity analysis of biochemical networks. *The Journal of Physical Chemistry B*, 108(3):1143–1152, 2004. doi:10.1021/jp036567u.

[23] Brian Ingalls. Sensitivity analysis: from model parameters to system behaviour. *Essays in Biochemistry*, 45:177–194, 09 2008. ISSN 0071-1365. doi:10.1042/bse0450177.

[24] Brian P Ingalls. A control-theoretic interpretation of metabolic control analysis. In Pablo A Iglesias and Brian P Ingalls, editors, *Control theory and systems biology*, chapter 8, pages 145–168. MIT Press, Cambridge, MA, 2010.

[25] M. Khammash and H. El-Samad. Systems biology: from physiology to gene regulation. *Control Systems, IEEE*, 24(4):62–76, 2004. ISSN 1066-033X. doi:10.1109/MCS.2004.1316654.

[26] Mustafa Khammash. An engineering viewpoint on biological robustness. *BMC Biology*, 14(1):22, 2016. ISSN 1741-7007. doi:10.1186/s12915-016-0241-x.

[27] Q. Peter He and Jin Wang. Application of systems engineering principles and techniques in biological big data analytics: A review. *Processes*, 8(8), 2020. ISSN 2227-9717. doi:10.3390/pr8080951.

[28] Peter J. Gawthrop and Michael Pan. Network thermodynamics of biological systems: A bond graph approach. *Mathematical Biosciences*, 352:108899, 2022. ISSN 0025-5564. doi:https://doi.org/10.1016/j.mbs.2022.108899.

[29] Michael Pan, Peter J. Gawthrop, Kenneth Tran, Joseph Cursons, and Edmund J. Crampin. A thermodynamic framework for modelling membrane transporters. *Journal of Theoretical Biology*, 481:10–23, Nov 2019. ISSN 0022-5193. doi:10.1016/j.jtbi.2018.09.034.

[30] H. M. Paynter. *Analysis and Design of Engineering Systems*. MIT Press, Cambridge, Mass., 1961.

[31] H.M. Paynter. An epistemic prehistory of bond graphs. In P.C. Breedveld and G. Dauphin-Tanguy, editors, *Bond Graphs for Engineers*, pages 3–17. North-Holland, Amsterdam, 1992.

[32] P. E. Wellstead. *Introduction to Physical System Modelling*. Academic Press, 1979.

[33] P. J. Gawthrop and L. P. S. Smith. *Metamodelling: Bond Graphs and Dynamic Systems*. Prentice Hall, Hemel Hempstead, Herts, England., 1996. ISBN 0-13-489824-9. doi:10.5281/zenodo.6998395.

[34] Amalendu Mukherjee, Ranjit Karmaker, and Arun Kumar Samantaray. *Bond Graph in Modeling, Simulation and Fault Indentification*. I.K. International, New Delhi,, 2006.

[35] Dean C Karnopp, Donald L Margolis, and Ronald C Rosenberg. *System Dynamics: Modeling, Simulation, and Control of Mechatronic Systems*. John Wiley & Sons, Hoboken, New Jersey, 5th edition, 2012. ISBN 978-0470889084.

[36] Peter J Gawthrop and Geraint P Bevan. Bond-graph modeling: A tutorial introduction for control engineers. *IEEE Control Systems Magazine*, 27(2):24–45, April 2007. doi:10.1109/MCS.2007.338279.

[37] George Oster, Alan Perelson, and Aharon Katchalsky. Network thermodynamics. *Nature*, 234:393–399, December 1971. doi:10.1038/234393a0.

[38] George F. Oster, Alan S. Perelson, and Aharon Katchalsky. Network thermodynamics: dynamic modelling of biophysical systems. *Quarterly Reviews of Biophysics*, 6(01):1–134, 1973. doi:10.1017/S0033583500000081.

[39] A.S. Perelson. Network thermodynamics. an overview. *Biophysical Journal*, 15(7):667 – 685, 1975. ISSN 0006-3495. doi:10.1016/S0006-3495(75)85847-4.

[40] Peter J. Gawthrop and Edmund J. Crampin. Energy-based analysis of biochemical cycles using bond graphs. *Proceedings of the Royal Society A: Mathematical, Physical and Engineering Science*, 470(2171):1–25, 2014. doi:10.1098/rspa.2014.0459.

[41] P. J. Gawthrop and E. J. Crampin. Modular bond-graph modelling and analysis of biomolecular systems. *IET Systems Biology*, 10(5):187–201, October 2016. ISSN 1751-8849. doi:10.1049/iet-syb.2015.0083.

[42] P. J. Gawthrop, I. Siekmann, T. Kameneva, S. Saha, M. R. Ibbotson, and E. J. Crampin. Bond graph modelling of chemoelectrical energy transduction. *IET Systems Biology*, 11 (5):127–138, 2017. ISSN 1751-8849. doi:10.1049/iet-syb.2017.0006.

[43] P. Gawthrop and E. J. Crampin. Bond graph representation of chemical reaction networks. *IEEE Transactions on NanoBioscience*, 17(4):449–455, October 2018. ISSN 1536-1241. doi:10.1109/TNB.2018.2876391.

[44] Michael Pan, Peter J. Gawthrop, Joseph Cursons, and Edmund J. Crampin. Modular assembly of dynamic models in systems biology. *PLOS Computational Biology*, 17(10): e1009513, Oct 2021. doi:10.1371/journal.pcbi.1009513.

[45] Peter J. Gawthrop, Michael Pan, and Edmund J. Crampin. Modular dynamic biomolecular modelling with bond graphs: the unification of stoichiometry, thermodynamics, kinetics and data. *Journal of The Royal Society Interface*, 18(181):20210478, 2021. doi:10.1098/rsif.2021.0478.

[46] Peter J. Gawthrop and Michael Pan. Energy-based advection modelling using bond graphs. *Journal of The Royal Society Interface*, 19(195):20220492, 2022. doi:10.1098/rsif.2022.0492.

[47] P.H. Roe and J.U. Thoma. A new Bond Graph approach to sensitivity analysis. In I Troch and F. Breitenecker, editors, *Proceedings of the 3rd IMACS Symposium on Mathematical Modelling*, pages 743–746, Vienna, Austria, February 2000. ARGESIM. ISBN 3-901608-X.

[48] Peter J Gawthrop. Sensitivity bond graphs. *Journal of the Franklin Institute*, 337(7):907–922, November 2000. doi:10.1016/S0016-0032(00)00052-1.

[49] Peter J. Gawthrop and Eric Ronco. Estimation and control of mechatronic systems using sensitivity bond graphs. *Control Engineering Practice*, 8(11):1237–1248, November 2000. doi:10.1016/S0967-0661(00)00062-9.

[50] G. Guardabassi, A. Locatelli, and S. Rinaldi. Structural properties of sensitivity systems. *Journal of the Franklin Institute*, 294(4):241–248, 1972. ISSN 0016-0032. doi:https://doi.org/10.1016/0016-0032(72)90022-1.

[51] Tina Toni, David Welch, Natalja Strelkowa, Andreas Ipsen, and Michael P. H. Stumpf. Approximate bayesian computation scheme for parameter inference and model selection in dynamical systems. *Journal of The Royal Society Interface*, 6(31):187–202, Jul 2008.

[52] P. J. Gawthrop. Energy-based modeling of the feedback control of biomolecular systems with cyclic flow modulation. *IEEE Transactions on NanoBioscience*, 20(2):183–192, April 2021. ISSN 1558-2639. doi:10.1109/TNB.2021.3058440.

[53] Peter Atkins and Julio de Paula. *Physical Chemistry for the Life Sciences*. Oxford University Press, 2nd edition, 2011.

[54] Pierre Van Rysselberghe. Reaction rates and affinities. *The Journal of Chemical Physics*, 29(3):640–642, 1958. doi:10.1063/1.1744552.

[55] Ryan N Gutenkunst, Joshua J Waterfall, Fergal P Casey, Kevin S Brown, Christopher R Myers, and James P Sethna. Universally sloppy parameter sensitivities in systems biology models. *PLoS Comput Biol*, 3(10):1–8, 10 2007. doi:10.1371/journal.pcbi.0030189.

[56] Peter J. Gawthrop, Joseph Cursons, and Edmund J. Crampin. Hierarchical bond graph modelling of biochemical networks. *Proceedings of the Royal Society A: Mathematical, Physical and Engineering Sciences*, 471(2184):1–23, 2015. ISSN 1364-5021. doi:10.1098/rspa.2015.0642.

[57] Matteo Polettini and Massimiliano Esposito. Irreversible thermodynamics of open chemical networks. I. Emergent cycles and broken conservation laws. *The Journal of Chemical Physics*, 141(2):024117, 2014. doi:10.1063/1.4886396.

[58] P. J. Gawthrop. Bond graph modeling of chemiosmotic biomolecular energy transduction. *IEEE Transactions on NanoBioscience*, 16(3):177–188, April 2017. ISSN 1536-1241. doi:10.1109/TNB.2017.2674683.

[59] Dean Karnopp. Power and energy in linearized physical systems. *Journal of the Franklin Institute*, 303(1):85 – 98, 1977. ISSN 0016-0032. doi:10.1016/0016-0032(77)90078-3.

[60] H. Kwakernaak and R. Sivan. *Linear Optimal Control Systems*. Wiley, New York, 1972.

[61] T. Kailath. *Linear Systems*. Prentice-Hall, Englewood Cliffs, 1980.

[62] C.S. Hsu and D. Hou. Reducing unstable linear control systems via real schur transformation. *Electronics Letters*, 27:984–986(2), May 1991. ISSN 0013-5194. doi:10.1049/el:19910614.

[63] Athel Cornish-Bowden. *Fundamentals of enzyme kinetics*. Wiley-Blackwell, London, 4th edition, 2013. ISBN 978-3-527-33074-4.

[64] Reginald H. Garrett and Charles M. Grisham. *Biochemistry*. Cengage Learning, Boston, MA, 6th edition, 2017.

[65] Jeremy M. Berg, John L. Tymoczko, Gregory J. Gatto, and Lubert Stryer. *Biochemistry*. W.H. Freeman, New York, ninth edition, 2019. ISBN 978-1-319-11465-7.

[66] Matthew G. Vander Heiden, Lewis C. Cantley, and Craig B. Thompson. Understanding the Warburg effect: The metabolic requirements of cell proliferation. *Science*, 324(5930): 1029–1033, 2009. ISSN 0036-8075. doi:10.1126/science.1160809.

[67] Krushna C. Patra and Nissim Hay. The pentose phosphate pathway and cancer. *Trends in Biochemical Sciences*, 39(8):347 – 354, 2014. ISSN 0968-0004. doi:10.1016/j.tibs.2014.06.005.

[68] J. Orth, R. Fleming, and B. Palsson. Reconstruction and use of microbial metabolic networks: the core escherichia coli metabolic model as an educational guide. *EcoSal Plus*, 2010. doi:10.1128/ecosalplus.10.2.1.

[69] Bernhard Palsson. *Systems Biology: Constraint-Based Reconstruction and Analysis*. Cambridge University Press, Cambridge, 2015.

[70] Junyoung O. Park, Sara A. Rubin, Yi-Fan Xu, Daniel Amador-Noguez, Jing Fan, Tomer Shlomi, and Joshua D. Rabinowitz. Metabolite concentrations, fluxes and free energies imply efficient enzyme usage. *Nat Chem Biol*, 12(7):482–489, Jul 2016. ISSN 1552-4450. doi:10.1038/nchembio.2077.

[71] Sawyer Fuller, Ben Greiner, Jason Moore, Richard Murray, Rene van Paassen, and Rory Yorke. The Python Control Systems Library (python-control). In *2021 60th IEEE Conference on Decision and Control (CDC)*, pages 4875–4881, Dec 2021. doi:10.1109/CDC45484.2021.9683368.

[72] Mengbo Li, Benjamin L. Parker, Evangeline Pearson, Benjamin Hunter, Jacob Cao, Yen Chin Koay, Oneka Guneratne, David E. James, Jean Yang, Sean Lal, and John F. O'Sullivan. Core functional nodes and sex-specific pathways in human ischaemic and dilated cardiomyopathy. *Nature Communications*, 11(1):2843, Jun 2020. ISSN 2041-1723. doi:10.1038/s41467-020-16584-z.

[73] Ann C. Babtie and Michael P. H. Stumpf. How to deal with parameters for whole-cell modelling. *Journal of The Royal Society Interface*, 14(133):20170237, Aug 2017. doi:10.1098/rsif.2017.0237.

[74] Gloria M. Monsalve-Bravo, Brodie A. J. Lawson, Christopher Drovandi, Kevin Burrage, Kevin S. Brown, Christopher M. Baker, Sarah A. Vollert, Kerrie Mengersen, Eve

McDonald-Madden, and Matthew P. Adams. Analysis of sloppiness in model simulations: Unveiling parameter uncertainty when mathematical models are fitted to data. *Science Advances*, 8(38):eabm5952, September 2022. ISSN 2375-2548. doi:10.1126/sciadv.abm5952.

[75] Subham Choudhury, Michael Moret, Pierre Salvy, Daniel Weilandt, Vassily Hatzimanikatis, and Ljubisa Miskovic. Reconstructing kinetic models for dynamical studies of metabolism using generative adversarial networks. *Nature Machine Intelligence*, 4:710–719, August 2022. ISSN 2522-5839. doi:10.1038/s42256-022-00519-y.

[76] Subham Choudhury, Bharath Narayanan, Michael Moret, Vassily Hatzimanikatis, and Ljubisa Miskovic. Generative machine learning produces kinetic models that accurately characterize intracellular metabolic states. *bioRxiv*, page 2023.02.21.529387, February 2023.

[77] Michael Ederer and Ernst Dieter Gilles. Thermodynamically feasible kinetic models of reaction networks. *Biophysical Journal*, 92(6):1846–1857, Mar 2007. ISSN 0006-3495. doi:10.1529/biophysj.106.094094.

[78] John C. Mason and Markus W. Covert. An energetic reformulation of kinetic rate laws enables scalable parameter estimation for biochemical networks. *Journal of Theoretical Biology*, 461:145–156, Jan 2019. ISSN 0022-5193. doi:10.1016/j.jtbi.2018.10.041.

[79] William M. Shaw, Hitoshi Yamauchi, Jack Mead, Glen-Oliver F. Gowers, David J. Bell, David Öling, Niklas Larsson, Mark Wigglesworth, Graham Ladds, and Tom Ellis. Engineering a model cell for rational tuning of gpcr signaling. *Cell*, 177(3):782–796, Apr 2019. ISSN 0092-8674. doi:10.1016/j.cell.2019.02.023.

[80] Robyn P. Araujo and Lance A. Liotta. The topological requirements for robust perfect adaptation in networks of any size. *Nature Communications*, 9(1757):1–12, May 2018. ISSN 2041-1723. doi:10.1038/s41467-018-04151-6.

[81] Robyn Araujo and Lance Liotta. Universal structures for embedded integral control in biological adaptation. *Research Square*, April 2022. doi:10.21203/rs.3.rs-1571178/v1.

[82] Joshua Forrest, Michael Pan, Edmund J. Crampin, Vijay Rajagopal, and Michael P. H. Stumpf. Energy dependence of signalling dynamics and robustness in bacterial two component systems. *bioRxiv*, page 2023.02.12.528212, February 2023.

[83] J. T. Locsei. Persistence of direction increases the drift velocity of run and tumble chemotaxis. *Journal of Mathematical Biology*, 55(1):41–60, July 2007. ISSN 1432-1416. doi:10.1007/s00285-007-0080-z.

[84] Shidong Song, Alexander F. Mason, Richard A. J. Post, Marco De Corato, Rafael Mestre, N. Amy Yewdall, Shoupeng Cao, Remco W. van der Hofstad, Samuel Sanchez, Loai K. E. A. Abdelmohsen, and Jan C. M. van Hest. Engineering transient dynamics of artificial cells by stochastic distribution of enzymes. *Nature Communications*, 12(6897):1–9, November 2021. ISSN 2041-1723. doi:10.1038/s41467-021-27229-0.